Diptera-specific Daedalus controls Zucchini endonucleolysis in piRNA biogenesis independent of exonucleases

Yuica Koga, Shigeki Hirakata, Mayu Negishi, Hiroya Yamazaki, and Mikiko C. Siomi*

Department of Biological Sciences, Graduate School of Science, The University of Tokyo, Tokyo 113-0032, Japan

*Correspondence: siomim@bs.s.u-tokyo.ac.jp

Summary

PIWI-interacting RNAs (piRNAs) protect germline genomes and maintain fertility by repressing transposons. Daedalus and Gasz act together as a mitochondrial scaffold for Armitage, a necessary factor for Zucchini-dependent piRNA processing. However, the mechanism underlying this function remains unclear. Here, we find that the requirements of Daedalus and Gasz in this process are different: Daedalus physically interacts with Armitage, whereas Gasz supports Daedalus to maintain its function. Daedalus binds to Armitage through two distinct regions, an extended coiled-coil identified in this study, and a sterile α motif (SAM). The former tethers Armitage to mitochondria, while the latter controls Zucchini endonucleolysis to define the length of piRNAs in an exonuclease-independent manner. piRNAs produced in the absence of Daedalus SAM do not exhibit full transposon silencing functionality. Daedalus is Diptera specific. Evolutionarily more complex species, such as mice, rely on exonucleases after Zuc processing to specify the length of piRNAs.

Keywords

Armitage, Daedalus, Gasz, piRNA, Zucchini, AmTEC, extended coiled-coil

Introduction

In *Drosophila* ovarian somatic cells (OSCs), the PIWI-interacting RNA (piRNA)-induced silencing complex (piRISC) assembles with one of the PIWI members, Piwi, in the cytoplasm.[1–4] piRISC then co-transcriptionally represses transposons in the nucleus. The vast majority of piRNAs in OSCs originate from the piRNA cluster, *flamenco* (*flam*).[5] The *flam* locus contains numerous transposon remnants, most of which have an orientation

35 opposite to the direction of transcription. Therefore, piRNAs can naturally hybridize to
36 target mRNAs through RNA–RNA base pairing.[5,6] After nuclear processing, including
37 splicing,[7] the *flam* transcripts are exported to the cytoplasm where they bind to female
38 sterile (1) Yb (Yb) via *cis*-elements embedded in the RNAs. This interaction induces the
39 assembly of non-membranous organelle Yb bodies through phase separation, which
40 accelerates subsequent steps in the piRNA processing.[8,9]

41 At this point, the *flam* transcripts are coarsely digested by an unknown factor,
42 generating numerous 5′ ends. Piwi binds one-to-one to these 5′ ends via the MID domain
43 and becomes the Piwi-piRISC precursor (pre-Piwi-piRISC).[10,11] Concomitantly, the RNA
44 helicase Armitage (Armi) binds to the complex, allowing pre-Piwi-piRISC to exit Yb
45 bodies and move to the mitochondrial surface where Zucchini (Zuc) awaits to process
46 the complex.[12] Zuc has a transmembrane (TM) region, which localizes Zuc to the outer
47 membrane of mitochondria.[13–16] After Zuc RNA cleavage releases mature Piwi-piRISC
48 from pre-Piwi-piRISC, nascent Piwi binds to the remaining piRNA precursor through its
49 5′ end, generating a new pre-Piwi-piRISC in Yb body-independent and Zuc-dependent
50 manners. This mechanism of sequential generation of Piwi-piRISC from a single piRNA
51 precursor is known as phasing.[17,18] Piwi-piRISC is then transported to the nucleus,[19]
52 where it associates with nascent transposon transcripts and suppresses transcription in
53 concert with multiple cofactors, such as Gtsf1/Asterix and Maelstrom.[20–27]

54 An RNAi-based gene screen performed in *Drosophila* ovaries identified many
55 factors acting in the piRNA pathway, including Gasz and Daedalus (Daed).[28] Both
56 proteins have a TM, like Zuc, and they form a heteromeric complex that acts in concert
57 with Armi to support Zuc cleavage in piRNA maturation.[12,29] However, the molecular
58 details of this process, especially the function of Daed, remain unclear.

In this study, we found that Daed interacts with Armi through two distinct regions, the extended coiled-coil (eCC) identified in this study, and the sterile α motif (SAM). We also show that Daed interacts with Gasz by forming a helical barrel using the two α-helixes present in each of Daed and Gasz. Through this interaction, Daed stabilizes Gasz, but not *vice versa*. Furthermore, we found that the Armi–Daed interaction through Daed eCC tethers Armi to mitochondria, while the Armi–Daed interaction through SAM controls Zuc endonucleolysis to specify the length of piRNAs in an exonuclease-independent manner. piRNAs produced in the absence of Daed SAM became atypically long and their function in transposon silencing was attenuated. Evolutionarily more complex species, such as mice, possess exonuclease, PNLDC1, but not Daed. Mouse piRNAs, which are atypically elongated in the absence of PNLDC1, do not exhibit full functionality in transposon silencing. These findings indicate that piRNA length specification, which is crucial for transposon repression, is conserved between species, but that the means of piRNA length specification differ between species.

Results

Daed and Gasz bind with each other via their respective eCC domains

According to the current model, the Daed–Gasz heterodimer tethers Armi bound to pre-Piwi-piRISC to mitochondria for Zuc-dependent piRNA processing.[12,29] In this study, we first predicted the higher-order structure of the Daed–Gasz heterodimer using AlphaFold2[30,31] (Figure 1A). This indicated that both Gasz and Daed have two α-helixes and that the coiled-coil structure composed of these four α-helixes is the center of the Daed–Gasz association (Figure 1B). Daed has SAM, coiled-coil (CC), and TM domains, and Gasz has ankyrin repeats (ARs), SAM, and TM domains.[12,29] The predicted

structures of Daed and Gasz showed that the second of the two α-helixes (Ala191–His235) of Daed roughly overlaps with the CC domain (Thr206–Ser234) and that the two α-helixes in Gasz (Phe345–Glu374 and Glu383–Ser412) are present between the SAM and TM domains (Figure 1C). The amino acid sequence-based prediction of the CC region[32] also roughly overlaps with the tandem α-helix regions (Figure S1A), supporting the AlphaFold2 prediction. We propose that the two tandem α-helixes present in both Gasz and Daed are referred to as extended coiled-coil (eCC) domains (Figure 1C).

The CC domain of Daed is the region that binds to Gasz.[29] To identify the region of Gasz responsible for binding to Daed we expressed deletion mutants of Gasz in OSCs lacking endogenous Gasz and then performed immunoprecipitation assays. Three of the Gasz deletion mutants, ΔAR1-3, which lacks the first three ARs, ΔAR4-6, which lacks the second three ARs, and ΔSAM, bound to Daed as efficiently as wild-type (WT) Gasz did, but the other mutant, Δα-H2, lacking the second α-helix of eCC did not (Figures 1D and S1B). These results indicate that the respective eCC domains of Daed and Gasz are responsible for the Daed–Gasz association, consistent with the predicted structure.

Daed stabilizes Gasz via protein–protein interaction

To verify whether Daed is required for piRNA biogenesis in cultured OSCs, we depleted intracellular Daed by RNA interference (RNAi) and conducted northern blotting. In control OSCs, both *idefix* piRNA (a representative nongenic piRNA) and *traffic jam* (*tj*) piRNA (a representative genic piRNA) were detected as expected (Figure S2A).[12] However, in the absence of Daed, their piRNA precursors (pre-piRNAs) accumulated aberrantly, while mature piRNAs were barely detected (Figure S2A), as in OSCs lacking Gasz.[12] This indicates that both Gasz and Daed are essential for piRNA maturation in OSCs.

107 Western blotting confirmed that RNAi was effective at depleting Daed and Gasz
108 in OSCs (Figure 2A). We also found that, when Daed was depleted, levels of Gasz were
109 also markedly reduced, but that levels of Daed were unchanged in the absence of Gasz
110 (Figures 2A and 2B). Such trends were not observed for their mRNA levels (Figure 2C).
111 These results indicate that Daed is required to stabilize Gasz at the protein level, but that
112 Daed is not dependent on Gasz for its stabilization.
113 To investigate which domain of Daed is involved in Gasz stabilization, two
114 deletion mutants of Daed, ΔSAM and ΔCC (part of the second α-helix of the eCC, see in
115 Figure 1C), were expressed in OSCs depleted of endogenous Daed. Levels of Gasz
116 were restored with expression of WT Daed and ΔSAM mutant Daed, but not with ΔCC
117 mutant Daed (Figure 2D). A previous study showed that Daed binds to Gasz via the CC
118 region[29] and together these findings indicate that the Daed–Gasz interaction via their
119 respective eCC domains is crucial for the stabilization of Gasz (Figure 2E). The Δα-H2
120 mutant of Gasz, which lacks the binding domain to Daed, was rather unstable in OSCs,
121 but this was not because of mRNA instability (Figure S2B), supporting the above notion.
122

123 **Daed alone or Gasz alone is insufficient to tether Armi to mitochondria**

124 Armi has at least two roles in piRNA biogenesis in OSCs; one is to transport nascent
125 Piwi to Yb bodies to promote pre-Piwi-piRISC assembly, and the other is to translocate
126 the complex from Yb bodies to mitochondria to promote Zuc-dependent piRNA
127 processing.[12,33] After this second role, Armi returns to the cytosol to repeat these
128 functions, although immunofluorescence shows that Armi appears to be a constant
129 resident of Yb bodies (Control, Figure 2F).[8,12] In the absence of Zuc, Armi signals merged
130 with mitochondrial signals {[I] Zuc knockdown (KD), Figure 2F}. This demonstrates

131 dynamic movement of Armi in OSCs and indicates that Armi remains on the
132 mitochondrial surface when loss of Zuc impairs piRNA maturation.[12] Results from
133 mitochondrial fractionation followed by western blotting were consistent with this
134 statement (Figures 2G and S2C).

135 We then depleted Daed in Zuc-lacking OSCs, where both Daed and Gasz
136 should be absent (Figure 2A). Under these circumstances, as expected, Armi was not
137 retained on mitochondria and appeared in Yb bodies ([II] Zuc KD + Daed KD, Figure 2F).
138 To restore the levels of both Daed and Gasz simultaneously, Flag-Daed was
139 exogenously expressed in the OSCs and western blotting confirmed the recovery of both
140 Daed and Gasz levels (Figures 2G and S2C). Immunofluorescence showed that Armi
141 re-localized to mitochondria ([III] Flag-Daed, Figure 2F). However, when Gasz was
142 forcibly expressed alone in the absence of Daed, Armi remained in Yb bodies ([IV] Flag-
143 Gasz, Figure 2F). A similar result was obtained in OSCs expressing only Daed ([V] Zuc
144 KD + Gasz KD, Figure 2F). These results indicate that Gasz alone or Daed alone is not
145 sufficient to tether Armi to mitochondria. In other words, both Daed and Gasz are
146 required to retain Armi on the mitochondrial surface for Zuc-dependent piRNA
147 processing. Hereafter, the Daed–Gasz heterodimer is referred to as the Armi
148 mitochondrial tethering complex (AmTEC). The behavior of Armi in OSCs under the
149 conditions described above is summarized in Figure S2D.

150

151 **Daed, but not Gasz, binds to Armi via two distinct sites**

152 We next predicted the higher-order structure of AmTEC bound with Armi (Figure 3A).
153 Notably, no significant interaction between Gasz and Armi was observed, but Daed and
154 Armi were bound at two distinct sites: The first site was through the first α-helix of eCC

155 (Phe144–Val177) (Figure 1C), which interacted with the N-terminal region of Armi
156 (Met1–Leu34) (Figures 3A, 3B, and S3A). The second interaction was between the SAM
157 domain of Daed (Figure 1C) and the C-terminal helicase (i.e., UPF1-like family) domain
158 of Armi (Figures 3A, 3C, and S3A).

159 To verify that the Armi–Daed interaction was via the Armi N-terminus (Figure
160 3B), recombinant WT Armi (WT-Flag) and its mutant lacking 34 N-terminal residues
161 (ΔN34-Flag) were subjected to pull-down assays with Daed (Daed ΔTM) as prey. The
162 Daed TM was removed because its inclusion interfered with protein preparation. Under
163 conditions where a negative control, Luciferase (Luc), showed no binding to Daed ΔTM,
164 Armi WT bound to Daed but Armi ΔN34 did not (Figure 3D). This confirms that Armi and
165 Daed interact through the 34 N-terminal residues of Armi. We have previously shown
166 that the Armi ΔN34 mutant (i.e., a shorter isoform of Armi) is unable to leave Yb bodies.[12]
167 The present analysis raises an alternative hypothesis; the Armi ΔN34 mutant may be
168 able to leave Yb bodies but not be tethered to mitochondria because of the absence of
169 Daed binding. This would explain why the shorter Armi isoform is inactive in piRNA
170 biogenesis in OSCs.

171 To verify the Armi–Daed interaction via the Armi UPF1-like helicase domain
172 (Figure 3C), three residues in the domain, Asp1015, Arg1026, and Arg1037 (D-R-R),
173 which appear to be key to the binding, were mutated to Lys-Glu-Glu (K-E-E) and
174 immunoprecipitation assays were conducted (Figure 3E). Quantification of the results
175 indicated that the Armi KEE mutant bound to Daed with approximately 34% of the binding
176 efficiency of WT Armi (Figure 3F). Meanwhile, the Armi ΔN34 mutant bound to Daed with
177 approximately 20% of the binding efficiency of WT Armi. Immunofluorescence showed
178 that the Armi ΔN34 mutant accumulated in Yb bodies more intensely than the KEE

179 mutant in Arm/Zuc-lacking OSCs (Figure 3G). For binding to Daed, Armi may be more
180 dependent on the N-terminal region than on the UPF1-like helicase domain.

181 A lack of Armi in OSCs severely disrupted piRNA production.[16,34] This was
182 almost fully rescued by the expression of WT Armi (Figure 3H). We next expressed the
183 ΔN34 or KEE mutants of Armi as alternatives to the WT. The ΔN34 mutant failed to
184 rescue the disruption to piRNA production, but the KEE mutant partially restored piRNA
185 biogenesis (Figures 3H, S3B and S3C). This supports the notion that the N-terminal
186 region of Armi is more important than the C-terminal helicase domain in piRNA
187 biogenesis in OSCs. The strength of the Armi–Daed interaction (Figure 3E) appears to
188 be positively correlated with the function of Armi.

189

190 **The two Armi–Daed associations differ in their functional contributions to piRNA**
191 **biogenesis**

192 piRNAs produced under conditions involving the Armi KEE mutant were notably
193 increased in length by several bases (Figure 3H). We therefore investigated whether a
194 similar phenomenon occurred under conditions involving the Daed ΔSAM mutant, given
195 that the SAM domain is the binding partner of the UPF1-like helicase domain of Armi.
196 Indeed, in cells expressing the Daed ΔSAM mutant as an alternative to endogenous
197 Daed, Piwi-bound piRNAs became several bases longer and their levels were lower than
198 those in cells expressing WT Daed, but higher compared with cells lacking endogenous
199 Daed (Figures 4A and S4A).

200 To examine how the lack of binding between Daed SAM and Armi UPF1-like
201 domain actually affects piRNA biogenesis, we sequenced and analyzed Piwi-bound
202 piRNAs in OSCs expressing Daed ΔSAM and compared the results with those from

203 OSCs expressing WT Daed (Figures 4A and S4A). This length distribution of piRNAs
204 was indeed shifted towards the longer fractions when they were produced in cells lacking
205 the Daed SAM domain (Figure 4B). This trend was also observed when piRNAs were
206 subdivided by target transposons (Figure S4B). In contrast, piRNA-mapped transposons
207 were essentially unchanged (Figure S4C). This seems reasonable given that piRNAs
208 are produced from *flam* in both cases. Furthermore, the 1U bias[5,35] and piRNA
209 phasing[17,18] were similarly observed in both libraries (Figures 4C and 4D). The β-
210 elimination experiments showed the 3′ ends of the piRNAs to be modified with 2′-*O*-
211 methylation in both cases, unlike Argonaute 1 (Ago1)-bound miRNAs (Figure 4E).[36,37]
212 It should be noted that non-negligible amounts of Piwi immunofluorescence
213 remained in the cytoplasm when Daed ΔSAM was expressed in OSCs lacking
214 endogenous Daed (Figure 4F). piRNA loading is essential for Piwi nuclear
215 localization.[19,33] Therefore, we next examined the piRNA binding status of cytoplasmic
216 and nuclear Piwi. In contrast to nuclear Piwi, which was bound to piRNAs even in the
217 long fraction, cytoplasmic Piwi was bound to few piRNAs (Figure S4D). This indicates
218 that piRNAs produced under the ΔSAM conditions can localize Piwi to the nucleus as
219 piRISC, regardless of length, but are insufficient to convert all Piwi to functional Piwi-
220 piRISC. Consistent with this, transposons were not fully repressed under such conditions
221 (Figures 4G and S4E). These results indicate that the Armi–Daed association via the
222 UPF1-like helicase domain of Armi and the SAM domain of Daed is influential in Piwi-
223 piRISC production and function, although less so than the other Armi–Daed association
224 involving the 34 N-terminal residues of Armi and the eCC domain of Daed.
225
226 **The Armi–Daed interaction via Daed SAM optimizes Zuc endonucleolysis for**

227 **piRNA-mediated transposon repression**

228 To explore the nature of ΔSAM piRNA extension, we selected the 50,000 piRNA 5′ end
229 positions common to the WT and ΔSAM and with high abundance in WT libraries (Figure
230 S4F) and analyzed them further. Heatmaps depicted with their 5′ end positions aligned
231 clearly indicate that ΔSAM piRNAs are more diverse in length. Many of them have some
232 extra bases at the 3′ ends (Figure 4H). This is consistent with the length distribution
233 shown in Figure 4A. There are also a few shorter piRNAs (Figure 4H). The relatively
234 small number of shorter piRNAs may be because of protection by Piwi.

235 To further analyze the effects of Daed SAM loss on piRNAs, we extracted
236 abundant 5′-end positions of 26- and 27-nucleotide (nt) piRNAs in the WT library, and
237 then these piRNAs were classified as “Unchanged” (51,833 positions) and “Elongated”
238 (53,258 positions) according to the absence or presence of 3′-end elongation. Both
239 piRNA groups maintained comparable phasing and +1U bias (i.e., 1U bias of piRNAs,
240 real and virtual, immediately following piRNAs verified to bind to Piwi[17,18]) (Figure S4G),
241 indicating that piRNA elongation caused by the loss of Daed SAM is caused by Zuc
242 endonucleolysis.

243 We next sorted piRNAs by their length and aligned them according to the 3′
244 ends of piRNAs. This showed that atypically long piRNAs of around 28–33 nt in the WT
245 library tended to have significantly low U bias near their 3′ ends (U depletion), just
246 upstream of the 5′ ends of the immediately downstream piRNAs, as reported previously
247 (yellow boxes in WT, Figure 4I).[18] This was interpreted as showing that when Zuc cannot
248 find U-rich regions in the piRNA precursors it waits to cleave the substrate until the U-
249 poor region has passed, thereby producing atypically long piRNAs. This also explains
250 why there were fewer 28–33-nt piRNAs in the WT library (Figure 4B). In contrast, there

251 was less notable “U depletion” in 28–33-nt ΔSAM piRNAs (yellow boxes in ΔSAM, Figure
252 4I). In addition, there was a substantial number of 28–33-nt piRNAs in the ΔSAM library
253 (Figure 4B). This indicates that when the Armi–Daed interaction is attenuated because
254 of a lack of Armi–Daed association via Daed SAM (and the UPF1-like helicase domain
255 of Armi), Zuc somehow produces these longer piRNAs more preferentially regardless of
256 the U content in the precursor sequences while maintaining the +1U bias.

257 We simulated the effect of Daed ΔSAM on piRNA production. First, the data
258 shown in Figure 4B were fitted to normal distributions. In parallel, we hypothetically
259 fragmented the sequence of the *flam* locus (21,629,891 to 21,792,731 on the X
260 chromosome; T was converted to U) into 163 piRNA precursors, starting at U and into
261 sizes of 1,000 nt or close to that size, and then simulated Zuc-dependent piRNA
262 production from their 5′ ends by assuming that Zuc cleavage occurs before U, produces
263 18–40-nt piRNAs, and follows the normal distributions for WT and ΔSAM. Sequence
264 analysis of the obtained piRNAs (25–34 nt) indicated that U depletion was observed in
265 simulations fitting the WT distribution, starting from 29 nt, but less so in simulations fitting
266 the ΔSAM distribution (Figure S4H). This indicates that Zuc can make Piwi-piRISC
267 without the rule of following U depletion, but that the level of piRISC is insufficient for
268 transposon repression.

269 We also sequenced and analyzed Piwi-bound piRNAs in OSCs expressing the
270 Armi KEE mutant or WT Armi (Figures 3H and S3B). We found that piRNAs in the Armi
271 KEE library were also several bases longer than the Armi WT piRNAs and retained 1U
272 bias (Figures S4I and S4J). Heatmaps showed that the KEE piRNAs also exhibited
273 characteristics of 3′ end elongation (Figure S4K). These results further support our notion
274 that the SAM domain of Daed and the UPF1-like helicase domain of Armi are the binding

275 partners and that the Armi–Daed interaction is indispensable to optimize Piwi-piRISC
276 maturation by Zuc and piRISC function in OSCs.
277
278 **Daed is Diptera-specific and controls Zuc cleavage in a Nibbler-independent**
279 **manner**
280 Armi and Gasz are widely conserved among species from invertebrates to vertebrates,
281 but Daed is unique to the Diptera order, which is composed of Brachycera suborder,
282 which includes *Drosophila* and other fly species, and Nematocera suborder which
283 includes mosquitoes (Figure 5A, S5A and S5B). In contrast, other species not belonging
284 Diptera order do not appear to have Daed orthologs.[38]
285 In mice, primary piRNA biogenesis occurs in the inter-mitochondrial cement,
286 where Armi homolog, MOV10L1, Gasz homolog, ASZ1, Zuc homolog, PLD6, and TDRD
287 proteins play a role in piRNA production: MOV10L1 binds to PIWI proteins (MILI, MIWI
288 and MIWI2) and piRNA precursors and contributes to piRNA biogenesis through its
289 helicase activity.[39,40] ASZ1 is essential for the production of MILI-bound piRNAs in mice[41]
290 and is thought to tether MOV10L1 to mitochondria, together with TDRD proteins, such
291 as TDRD1, to promote MIWI-piRISC production.[39,40]
292 We expressed both MOV10L1 and ASZ1 in OSCs and performed
293 immunoprecipitation. The MOV10L1–ASZ1 interaction was detected to a similar extent
294 in both normal OSCs and OSCs lacking intracellular Daed (Figures 5B and 5C).
295 Immunofluorescence confirmed this; the expression of ASZ1 was sufficient for the
296 mitochondrial localization of MOV10L1, independent of the presence of intracellular
297 Daed (Figure 5D). This indicates that the MOV10L1–ASZ1 interaction and MOV10L1
298 tethering is Daed-independent, while the Armi–Gasz interaction and Armi tethering in

299 *Drosophila* required Daed. These results also indicate that the Armi–Gasz association,
300 at least in OSCs, does not require other factors present in mouse testis. ASZ1 was stable
301 in OSCs lacking endogenous Daed (Figure 5C), unlike Gasz (Figure 2A), indicating that
302 the molecular system that actively degrades Gasz in the absence of Daed does not act
303 on ASZ1.

304 Why did *Drosophila* acquire Daed during evolution? In mice, poly(A)-specific
305 ribonuclease-like domain containing 1 (PNLDC1), a homolog of poly(A)-specific
306 ribonuclease (PARN), trims the 3′ ends of piRNAs and piRNAs are elongated after
307 PNLDC1 loss of function.[42,43] Mutation in PNLDC1 reduces LINE-1-targeting piRNAs and
308 mislocalizes MIWI2 to the cytoplasm, leading to LINE-1 derepression. This was nearly
309 equal to what we observed in this study with the *Drosophila* Daed ΔSAM mutant.
310 However, PNLDC1 is not conserved in the majority of Diptera order species.[44] Papi is
311 the *Drosophila* ortholog of TDRKH, which, in mice, acts as a scaffold for PNLDC1 and
312 whose functional inhibition causes piRNA elongation.[45,46] However, consistent with
313 previous studies using Papi mutant flies,[44] its depletion had little effect on piRNA length
314 in OSCs (Figure 5E).

315 The 3′-to-5′ exonuclease, Nibbler (Nbr), trims both miRNAs and piRNAs in
316 *Drosophila* and mosquitoes,[44,47–49] but the pre-piRNAs that undergo trimming are minor
317 in mosquitoes, and the loss of Nbr barely affected the length of Piwi-bound piRNAs in
318 the *Drosophila* ovary.[44] Our study confirmed this; namely, Nbr depletion in OSCs had
319 little effect on the piRNA length (Figure 5F). This indicates that Nbr may function in the
320 trimming of miRNAs, but not piRNAs, in OSCs. The lack of a marked increase in +1U
321 signal in piRNAs elongated in the Daed ΔSAM mutant (Figures 4D and S4G) also
322 supports this view.

323 In contrast, Armi D-R-R, which was essential for the regulation of Zuc cleavage
324 in *Drosophila*, is highly conserved in the fly species that lack PNLDC1/PARN and have
325 Daed (Figure S5C). These results indicate that *Drosophila,* and its closely related
326 species, may have acquired Daed after losing PNLDC1/PARN during evolution, and that
327 they may also have acquired the ability to produce mature piRNAs without further
328 trimming by exonucleases by allowing Armi to bind directly to Daed (Figure 5G).
329

330 **Discussion**

331 This study revealed that Daed and Gasz bind to each other via their eCC domains, both
332 of which are composed of two α-helixes that assemble into a stable helical barrel
333 consisting of all four of these α-helixes. When Daed lacks the second α-helix in the eCC
334 domain, the Daed–Gasz interaction is disrupted and Gasz becomes destabilized,
335 illustrating the importance of Daed in Gasz stabilization (Figure 2E). This also shows that
336 the intracellular level of Gasz is strictly regulated by the intracellular level of Daed,
337 indicating that OSCs do not tolerate the presence of Gasz alone. In contrast, OSCs do
338 tolerate the presence of Daed alone. However, Daed, in the absence of Gasz, failed to
339 anchor pre-Piwi-piRISC to mitochondria via Armi. Gasz is therefore complicit in the role
340 of Daed, although the contribution of Gasz to the direct binding of Daed to Armi appears
341 to be minimal.

342 Lack of binding through the Daed SAM did not completely abolish the Armi–
343 Daed association but resulted in aberrant Zuc function (Figure S3C). Under such
344 conditions, Piwi-bound piRNAs were atypically long because of extra bases at the 3′
345 ends, and there was no notable U depletion, a typical feature of piRNAs in normal OSCs.
346 In normal OSCs, atypically long piRNAs are produced only when piRNAs of typical sizes

347 cannot maintain the +1U bias. In contrast, in OSCs expressing Daed ΔSAM, Zuc shows
348 "relaxed selectivity" in terms of nucleotides and length and tends to produce longer
349 piRNAs, even under conditions where it can produce shorter (i.e., normal size) piRNAs
350 with the +1U bias, albeit in relatively small quantities. This could be because of the timing
351 of Zuc RNA cleavage was shifted slightly downstream of the precursor while the
352 preference for cleavage before U was conserved. Recombinant Zuc did not show U
353 selectivity,[15] indicating that, *in vivo*, Zuc may rely on a cofactor to confer U selectivity,
354 and that this cofactor may not require the Armi–Daed association to execute its function.

355 Interestingly, Piwi could accept those longer piRNAs produced under the ΔSAM
356 conditions and localized to the nucleus as Piwi-piRISC. At the same time, however,
357 nonnegligible amounts of Piwi remained in the cytoplasm because of the lack of piRNA
358 loading, which resulted in transposon derepression. This means that the ability of Daed
359 to interact with Armi via the SAM domain, in addition to the binding via the first α-helix in
360 the eCC domain, is essential not only to define the positions of Zuc cleavage, but also
361 to produce enough Piwi-piRISC for transposon repression in OSCs. It is worth noting
362 that no such regulatory factor has been identified to date.

363 Armi is unique in that it plays multiple roles in piRNA biogenesis. First, Armi
364 delivers unloaded Piwi to Yb bodies, facilitating the assembly of pre-Piwi-piRISC in these
365 organelles. In Yb bodies, Armi binds to pre-Piwi-piRISC and translocates the complex to
366 mitochondria. There, Armi anchors pre-Piwi-piRISC to the mitochondria by binding to
367 Daed. This allows Zuc to process pre-Piwi-piRISC into mature Piwi-piRISC. Armi is
368 therefore a factor that always accompanies Piwi and encourages it along the pathway to
369 develop into Piwi-piRISC.

370 Armi is an RNA helicase protein, and its RNA helicase activity is required to

371 avoid stochastic interactions with abundant mRNAs.[50] In contrast, up to this point, the
372 RNA helicase activity of Armi does not seem to be required for the piRNA precursors,
373 rather its activity would be inhibitory. However, in the absence of this activity, especially
374 for phasing, the sequential generation of Piwi-piRISC from a single piRNA precursor
375 would not occur. It is possible that an inhibitor of the RNA helicase activity of Armi is
376 present in OSCs and functions until phasing, but, upon binding to Armi, Daed would lose
377 its function allowing phasing to occur.

378 Animals that reproduce sexually retain the highly conserved piRNA mechanism
379 and use it to maintain their fertility by repressing transposons. However, the evolutionary
380 rate of many piRNA factors, including Armi, is rapid,[51,52] suggesting that these species
381 have adapted the machinery to their specific endogenous and exogenous environments.
382 Coevolution of piRNAs and transposons through host–pathogen arms races has been
383 proposed as a background to this process.[53] Although flies and mosquitoes belong to
384 the same Diptera order, the piRNA pathway factors are highly diverse.[54] On the other
385 hand, our observation that Daed is conserved among Diptera species may suggest the
386 importance of this factor in Dipteran piRNA biogenesis pathway where PNLDC1 is lost.
387

388 **Author contributions**

389 YK and MN performed biochemical experiments. YK, SH, and HY performed
390 bioinformatic analyses, computational structural prediction, simulation, and calculation.
391 MCS supervised and discussed the work and wrote the manuscript with the other authors.
392

393 **Acknowledgments**

394 We thank Y. Namba, Y.W. Iwasaki, H. Nishimasu, S. Kuraku, Y. Fukushima, T. Yasuda

for useful discussions, and T. Fujisawa, T. Kinoshita, and H. Ishizu for technical assistance with the biochemical analysis. This study was supported by MEXT KAKENHI Grant Numbers JP19H05466 (to MCS), JP22K15056 (to SH), JP23K14141 (to HY), and JP22KJ1122 (to YK). Some computations were performed on the NIG supercomputer at ROIS National Institute of Genetics.

Conflict of interest

The authors declare no competing interests.

Figure legends

Figure 1. Daed and Gasz interact via their respective eCC domains

(**A**) Predicted structure of the Daed-Gasz heterodimer by AlphaFold2. (**B**) Magnification of the region indicated by the dotted line box in (**A**). The structure is shown from two directions. (**C**) Domain structures of Daed and Gasz. Peptide sequences of eCCs of Daed and Gasz are also shown. (**D**) Immunoprecipitation (Flag IP) and western blotting show that one of the Gasz mutants, Δα-H2, fails to bind to Daed in OSCs lacking endogenous Gasz. Flag-Luc: negative control. *: Heavy chains. The domain structures Gasz WT and deletion mutants are also shown.

Figure 2. Daed stabilizes Gasz via interaction and both Daed and Gasz are essential for the mitochondrial tethering of Armi

(**A**) Western blotting shows the high efficiency of knockdown (KD) of Daed and Gasz in OSCs. Daed KD also destabilizes Gasz, but not *vice versa*. β-Tub: loading control. (**B**, **C**) The statistics of western blotting signals (n=3; **A**) and the mRNA expression levels of

419 *Daed* and *Gasz* upon Daed KD and Gasz KD. Signal intensities (**B**) or values (**C**) relative
420 to control (EGFP KD) were normalized with those of β-Tub or *rp49*, respectively, and
421 presented as mean values ± SE. **: $p<0.01$; ***: $p<0.005$; n.s.: $p>0.05$ [*t*-test (unpaired,
422 two-sided)]. (**D**) Western blotting showing the levels of endogenous Gasz and Flag-Daed
423 (WT and deletion mutants) in OSCs under each condition. β-Tub: loading control. The
424 domain structures of Daed WT and mutants are shown. (**E**) Model of Gasz stabilization
425 by Daed. (**F**) Subcellular localization of Armi (green) in OSCs under various conditions,
426 [I] to [V]. Mitochondria (mito) and Yb bodies (Yb; white arrowheads) are shown in
427 magenta. The signals of Flag-Gasz and Flag-Daed are shown in yellow. Images in the
428 same vertical row are identical cells. Control: normal OSCs. DAPI (blue): nuclei. Scale
429 bar 5 μm. (**G**) Western blotting shows the levels of endogenous Armi, Gasz, Daed, Flag-
430 Gasz (orange asterisk), and Flag-Daed (blue asterisk) in total lysates (total) and
431 mitochondrial fractions (mito) under conditions [I] to [VI]. For the efficiency of cell
432 fractionation, see Figure S2C.
433
434 **Figure 3. Daed interacts with Armi through two sites, each contributing differently**
435 **to piRNA biogenesis**
436 (**A**) The structure of the Armi–AmTEC complex predicted by AlphaFold2. Gray lines:
437 virtual lipid bilayers. The domain structures of Armi, Daed, and Gasz are also shown. (**B**)
438 Magnification of the "B" region in (**A**). The 34 N-terminal residues of Armi (N34) interacts
439 with the first α-helix of Daed eCC. (**C**) Magnification of the "C" region in (**A**). The Armi
440 UPF1-like helicase domain interacts with Daed SAM. Asp1015, Arg1026, and Arg1037
441 of Armi are shown in blue. (**D**) *In vitro* pull-down assays show Armi WT-Flag, but not
442 Armi ΔN34-Flag, binding to Daed (Daed ΔTM-His). Luc-Flag: negative control. *: Heavy

443 and light chains. (**E**) Immunoprecipitation (Flag IP) and western blotting show the
444 amounts of endogenous Daed co-immunoprecipitated with Armi WT-Flag, ΔN34-Flag,
445 and KEE-Flag. Luc-Flag: negative control. The domain structures of Armi WT and its
446 mutants are shown below. Asp1015, Arg1026, and Arg1037 mutated in the KEE mutant
447 are also shown. The peptide sequence of Armi is shown in Figure S3A. (**F**) The statistics
448 of western blotting signals (n=3; **E**). The signals of Daed were normalized with those of
449 Armi and presented as mean values ± SE. *: p <0.05; ***: p <0.005 [t-test (unpaired,
450 two-sided)]. (**G**) Subcellular localization of Armi WT, ΔN34, and KEE (green) in OSCs
451 lacking endogenous Zuc (Zuc KD) and Armi (Armi KD). Mitochondria (mito; for WT and
452 KEE) and Yb bodies (Yb, white arrowhead; for ΔN34) are shown in magenta. Images in
453 the same vertical row are identical cells. DAPI (blue): nuclei. Scale bar: 5 μm. (**H**) Piwi-
454 bound piRNAs obtained under each condition. Signal intensities (n=3) are normalized as
455 a percentage of the total. The mean (line) and standard deviation (shadow) are shown.
456 The amount of Piwi in each sample is shown at the bottom.
457
458 **Figure 4. The loss of Armi–Daed interaction via Daed SAM obscures Zuc cleavage**
459 **and impairs Piwi-piRISC function**
460 (**A**) Piwi-bound piRNAs obtained under each condition. Signal intensities (n=3) are
461 normalized as a percentage of the total. The mean (line) and standard deviation
462 (shadow) are shown. The amount of Piwi in each sample is shown at the bottom. (**B**)
463 Length distribution of piRNAs (18–40 nt) in Daed WT (green) and ΔSAM (red) libraries
464 (n=3), presented as mean values ± SE. (**C**) Sequence logos representing 11 nt from the
465 5′ end of piRNAs in Daed WT and ΔSAM libraries. (**D**) Heatmaps showing 3′ end counts
466 of piRNAs mapped around the 10,000 most abundant piRNA 5′ ends (lower) and its

467 binary histograms (upper) in Daed WT (left) and ΔSAM (right). (**E**) β-elimination assays.
468 Piwi-bound piRNAs in Daed KD OSCs expressing Daed WT and ΔSAM are shown.
469 Ago1-bound miRNAs are used as positive controls. (**F**) Subcellular localization of
470 endogenous Piwi (green) in Daed KD OSCs expressing Daed WT and ΔSAM (magenta).
471 DAPI (blue): nuclei. Scale bar: 5 μm. (**G**) The expression levels of transposons (*mdg1*,
472 *tabor*, *412*, and *stalker2*) in control OSCs (dark gray), Daed-lacking OSCs (Daed KD;
473 light gray), Flag-Daed WT rescued (WT; green) or Flag-Daed ΔSAM rescued cells
474 (ΔSAM; red) (n=5). Values relative to the control (EGFP KD) were normalized to *rp49*
475 and presented as mean values ± SE **: $p < 0.01$; n.s.: $p > 0.05$ [Wilcoxon rank sum exact
476 test (two-sided)]. (**H**) Heatmaps showing the frequency of the 3′ end positions (red)
477 corresponding to each 5′ end of piRNAs in Daed WT (upper) and ΔSAM (lower) libraries.
478 The 50,000 piRNA 5′ end positions common to both libraries and most abundant in the
479 WT library were used for analysis. (**I**) Sequence logos. piRNAs were sorted by their
480 lengths and aligned according to the 3′ end of the piRNAs (black arrowhead) and its
481 immediately downstream nucleotide is highlighted in green. The U depletion found in 28–
482 33-nt piRNAs in the WT library and the equivalent regions in ΔSAM are highlighted in
483 yellow.
484
485 **Figure 5. Daed is fly-specific and controls Zuc cleavage in a Nbr-independent manner**
486 (**A**) Protein conservation state of Armi, Gasz, Daed, PNLDC1, Papi, and Nbr in *D.*
487 *melanogaster* and other species. (**B**, **C**) Immunoprecipitation (Flag IP) and western
488 blotting show Myc-ASZ1 binds to MOV10L1 in normal (**B**) and Daed-depleted OSCs (**C**).
489 Luc-Flag: negative control. (**D**) Subcellular localization of Myc-ASZ1 alone or MOV10L1-
490 Flag (green) with Myc-ASZ1 (yellow) in normal (left two row) and Daed-depleted OSCs

491 (right two row). Mitochondria (mito) are shown in magenta. Images in the same vertical
492 row are identical cells. DAPI (blue): nuclei. Scale bar: 5 μm. (**E**, **F**) The efficiency of Papi
493 KD (upper) and Nbr KD (lower) (n=3). Piwi-bound piRNAs in control and Papi-KD (upper)
494 and Nbr-KD OSCs (lower). The amount of Piwi in each sample is also shown. (**G**) Model
495 proposed in this study. Diptera species acquired Daed instead of PNLDC1/PARN during
496 evolution; Daed and Gasz form AmTAC, which stably tethers Armi to the mitochondrial
497 surface via two sites. This allows Zuc to define the length of piRNAs without relying on
498 exonucleases such as PNLDC1/PARN or Nbr. In contrast, in mice, MOV10L1/Armi is
499 tethered solely by ASZ1/Gasz. In this case, Zuc cleavage does not specify piRNA length;
500 therefore, trimming by exonucleases such as PNLDC1/PARN is required after Zuc
501 processing. Blue arrowhead: Zuc cleavage.
502
503 **STAR★Methods**
504 Key resources table

REAGENT or RESOURCE	SOURCE	IDENTIFIER
Antibodies		
Mouse monoclonal antibody Anti-Daed	This study	P3F10
Mouse monoclonal antibody anti-Gasz	Yamashiro et al.[12]	1H7
Mouse monoclonal antibody anti-Armi	Saito et al.[16]	2F8A9
Mouse monoclonal antibody anti-Piwi	Saito et al.[35]	3G11
Mouse monoclonal antibody anti-Piwi	Saito et al.[35]	4D2
Mouse monoclonal antibody anti-Yb	Murota et al.[55]	1G2H3
Mouse monoclonal antibody anti-Ago1	Okamura et al.[56]	1B8
Mouse monoclonal antibody anti-β-Tub	Developmental Studies Hybridoma Bank	Cat#E7; RRID: AB_528499
HSP60 antibody, Clone LK1	StressMarq Biosciences	Cat# SMC-110 (also SMC-110B), RRID:AB_2121277

Anti-Histon H3 antibody – Nuclear Loading Control and ChIP grade	abcam	Cat# ab1791, RRID:AB_302613
Monoclonal anti-Flag M2 antibody	Sigma-Aldrich	Cat# F3165, RRID:AB_259529
Anti-Flag antibody produces in rabbit	Sigma-Aldrich	Cat# F7425, RRID:AB_439687
Anti-c-Myc antibody produces in rabbit	Sigma-Aldrich	Cat# C3956, RRID:AB_439680
anti-mouse IgG (H+L) HRP	Cappel	55558
anti-rabbit IgG HRP-linked	Cell Signaling Technology	Cat#7074, RRID: AB_2099233
Alexa Fluor 488 goat anti-mouse IgG1 antibody	Thermo Fisher Scientific	Cat#A-21121; RRID: AB_2535764
Alexa Fluor 488 goat anti-mouse IgG2b antibody	Thermo Fisher Scientific	Cat# A-21141 (also A21141), RRID:AB_141626
Alexa Fluor 555 goat anti-mouse IgG1 antibody	Thermo Fisher Scientific	Cat#A-21127; RRID: AB_2535769
Alexa Fluor 555 goat anti-mouse IgG2b antibody	Thermo Fisher Scientific	Cat# A21147, RRID:AB_1500897
Alexa Fluor 633 goat anti-rabbit IgG (H+L) antibody	Thermo Fisher Scientific	Cat# A-21070 (also A21070), RRID:AB_2535731
Bacterial and virus strains		
Escherichia coli Rosetta 2 (DE3)	Novagen	Cat#71397
Chemicals, peptides, and recombinant proteins		
Shields and Sang M3 Insect Medium w/ L-Glutamine	USBiological	Cat#S1013
Fetal Bovine Serum	NICHIREI	Cat#173012
NEBuilder HiFi DNA Assembly Master Mix	New England Biolabs	Cat#E2621X
Ligation high ver.2	Toyobo	Cat#LGK-201
Glutathione Sepharose 4B	Cytiva	Cat#17-0756-01
Phosphate-buffered saline	FUJIFILM Wako Pure Chemical	Cat#048-29805
Thiophilic-Superflow Resin	Clontech	Cat#Z5616N
ClearTrans SP PVDF membranes	Fujifilm Wako Pure Chemical	Cat#033-22453
Clarity Western ECL Substrate	Bio-Rad	Cat#170506
Dynabeads Protein G	Thermo Fisher Scientific	Cat#10009D
RNasin Plus Ribonuclease Inhibitor	Promega	Cat#N2615
T4 Polynucleotide Kinase	New England Biolabs	Cat#M0201L

ISOGEN II	FUJIFILM Wako Pure Chemical	Cat#311-07361
Hybond-N membrane	Cytiva	Cat#RPN303N
VECTASHIELD Antifade Mounting Medium with DAPI	VECTOR LABORATORIES	Cat#H-1200
MitoTracker Orange CMXRos	Thermo Fisher Scientific	Cat#M-7510
SYBR Gold Nucleic Acid Gel Stain	Thermo Fisher Scientific	Cat#S11494
TURBO DNase	Life Technologies	Cat#AM2239
ReverTra Ace qPCR RT master mix	Toyobo	Cat#TYFSQ201
cOmplete ULTRA Tablets, EDTA-free, Protease Inhibitor Cocktail	Roche	Cat#6538282001
RNase A	Roche	Cat#10109142001
Critical commercial assays		
Nucleofector 96-well Shuttle device	Lonza	Cat#AAF-1003S
Nucleofector 2b device	Lonza	Cat#AAB-1001
ChemiDoc XRS Plus System	Bio-Rad	Cat#1708265J1PC
LSM980 laser scanning confocal microscope	Carl Zeiss	Cat#LSM980
StepOnePlus Real-Time PCR system	Thermo Fisher Scientific	Cat#4376598
MiSeq	Illumina	Cat#SY-410-1003
SF Cell Line 96-well Nucleofector Kit	Lonza	Cat#V4SC-3096
QIAseq FastSelect-rRNA Fly Kit	QIAGEN	Cat#333262
PowerUp SYBR Green Master Mix	Thermo Fisher Scientific	Cat# A25743
MiSeq Reagent Kit v3	Illumina	Cat#MS-102-3001
Deposited data		
Raw sequencing data	This paper	GEO: GSExxxxxx
Experimental models: Cell lines		
OSC	Saito et al.[33]	N/A
Oligonucleotides		
Primer sequences	Table S1	N/A
siRNA sequences	Table S2	N/A
Probe sequences	Table S3	N/A
qPCR primer sequences	Table S4	N/A
Recombinant DNA		
pGEX	Cytiva	Cat#28-9546-48
pAc-Flag-Daed WT and mutants	This study	N/A

pAc-Flag-Armi WT	Ishizu et al.[50]	N/A
pAc-Flag-Gasz WT	Yamashiro et al.[12]	N/A
pAc-Flag-Gasz mutants	This study	N/A
pAc-Armi WT-Flag	Yamashiro et al.[12]	N/A
pAc-Armi ΔN34-Flag	Yamashiro et al.[12]	N/A
pAc-Armi KEE-Flag	This study	N/A
pAc-Myc-Luc	gift from H. Ishizu	N/A
pAc- Luc-Flag	Yamashiro et al.[12]	N/A
pAc-Flag-Luc	This study	N/A
pAc-MOV10L1-Flag	This study	N/A
pAc-Myc-ASZ1	This study	N/A
Software and algorithms		
Python (Ver. 3.8.8)	Van Rossum & Drake[57]	RRID:SCR_008394;https://www.python.org
Numpy (Ver. 1.20.1)	Harris et al.[58]	RRID:SCR_008633; https://numpy.org/ja/
Scipy (Ver. 1.6.2)	Virtanen et al.[59]	RRID:SCR_008058; https://scipy.org
Pandas (Ver. 1.2.4)	McKinney[60]	RRID:SCR_018214;https://pandas.pydata.org
R (Ver. 4.3.1)	R Development Core Team[61]	RRID:SCR_001905;https://www.r-project.org
Cutadapt (Ver. 4.0)	Martin[62]	RRID:SCR_011841;https://cutadapt.readthedocs.io/en/stable/
STAR (Ver.2.7.8a)	Dobin et al.[63]	RRID:SCR_004463;https://github.com/alexdobin/STAR
HTSeq (Ver. 0.9.1)	Anders et al.[64]	RRID:SCR_005514;https://htseq.readthedocs.io/en/latest/
bedtools (Ver. 2.30.0)	Quinlan & Hall[65]	RRID:SCR_006646;https://bedtools.readthedocs.io/en/latest/
SAMtools (Ver. 1.9)	Li et al.[66]	RRID:SCR_002105;http://www.htslib.org
deepTools (Ver. 3.3.2)	Ramírez et al.[67]	RRID:SCR_016366;https://deeptools.readthedocs.io/en/develop/
wigToBigWig (Ver. 357)	UCSC	https://www.encodeproject.org/software/wigtobigwig/

ggseqlogo	Wagih.[68]	https://omarwagih.github.io/ggseqlogo/
RSeQC (Ver. 2.6.4)	Wang et al.[69]	RRID:SCR_005275;https://rseqc.sourceforge.net
Fiji (Ver. 2.0.0-rc-69/1.52p)	Schneider et al.[70]	RRID:SCR_002285; https://fiji.sc
AlphaFold (Ver. 2.3)	Jumper et al.[31]	https://github.com/google-deepmind/alphafold
UCSF ChimeraX (Ver. 1.6.1)	Pettersen et al.[71]	RRID:SCR_015872;https://www.cgl.ucsf.edu/chimerax/
ISOLDE (Ver. 1.6)	Croll[72]	https://tristanic.github.io/isolde/
CLUSTAL Omega	Madeira et al.[73]	RRID:SCR_001591;https://www.ebi.ac.uk/jdispatcher/msa/clustalo
iTOL (Ver. 6.9)	Letunic & Bork[74]	RRID:SCR_018174;https://itol.embl.de
seaborn (Ver. 0.12.2)	Waskom et al.[75]	https://seaborn.pydata.org
ESPript (Ver. 3.0)	Robert & Gouet[76]	https://espript.ibcp.fr
MEGA11	Tamura et al.[77]	RRID:SCR_023017; https://www.megasoftware.net/

Resource availability

Lead contact

Further information and requests for resources and reagents should be directed to and will be fulfilled by the lead contact, Mikiko C. Siomi (siomim@bs.s.u-tokyo.ac.jp).

Materials availability

Plasmids and antibodies generated in this study will be shared by the lead contact upon request.

Data and code availability

The data supporting the findings of this study are available from the corresponding authors upon reasonable request. The datasets produced in this study are available in the following databases: RNA-Seq data: Gene Expression Omnibus GSExxxxxx

517 (https://www.ncbi.nlm.nih.gov/geo/query/acc.cgi?acc=GSExxxxxx).

518 **Experimental model and study participant details**

519 OSCs were cultured at 26°C in Shields and Sang M3 medium (USBiological)
520 supplemented with 10% fetal bovine serum (FBS, NICHIREI), 0.6 mg/mL glutathione, 10
521 mU/mL insulin, and 10% fly extract.[8]

522

523 **Method details**

524 **Plasmid construction**

525 The Daed coding region was amplified from total OSC RNAs by RT-PCR and inserted
526 into pAc-Flag-Armi WT[50] by substituting the Armi coding region using NEBuilder HiFi
527 DNA Assembly Master Mix (New England Biolabs). RNAi-resistant Daed WT and its
528 ΔSAM and ΔCC mutants were generated by inverse PCR, according to the domain
529 structures described in a previous study.[29] To construct the expression vector for GST-
530 Daed ΔTM-His, corresponding coding regions of Daed were cloned into pGEX, after
531 which a His-Tag was added to the C-terminal by inverse PCR. RNAi-resistant Flag-Gasz
532 mutants (ΔAR1-3, ΔAR4-6, ΔSAM, and Δα-H2) were generated by inverse PCR using
533 RNAi-resistant Flag-Gasz WT vector[12] as a template. Vectors for RNAi-resistant Armi
534 WT-Flag and its ΔN34 mutant were previously constructed.[12] The Armi KEE-Flag mutant
535 was produced by inverse PCR using RNAi-resistant Armi WT-Flag vector as a template.
536 The Flag-Luc expression vector was generated from pAc-Myc-Luc (a gift from H. Ishizu)
537 by substituting Myc with 3×Flag. The primers used are shown in Table S1. The MOV10L1
538 and ASZ1 coding region was amplified from total mouse ovary RNAs by RT-PCR and
539 inserted into pAc-Armi WT-Flag and Myc-Daed WT by substituting original coding
540 regions.

541

542 **RNAi and transfection**

543 To initiate RNAi, 5.0 × 10^6 OSCs were mixed with 200 pmol of siRNAs in 20 μL of Solution
544 SF of the Cell Line Nucleofector Kit SF (Lonza Bioscience) and electroporation was
545 performed using a Nucleofector 96-well Shuttle device (Lonza Bioscience). For plasmid
546 transfection or plasmid/siRNA co-transfection, 1.5 × 10^7 OSCs were mixed with 1.5–10
547 μg of plasmids with or without 600 pmol of siRNAs in 100 μL of transfection buffer [180
548 mM sodium phosphate buffer for Church and Gilbert hybridization (pH 7.2), 5 mM KCl,
549 15 mM $MgCl_2$, and 50 mM D-mannitol] modified from a previous report,[78] and
550 electroporation was performed by a Nucleofector 2b device (Lonza Bioscience). Cells
551 were transfected with siRNAs twice with a 48-h interval. For rescue assays, endogenous
552 genes were depleted by RNAi and plasmids and siRNAs were introduced into the cells
553 after 48 h of culture. Cells were harvested after another 48 h of culture. For
554 immunofluorescence in Figure 2F, 500 pmol of siRNAs were used for RNAi and
555 plasmid/siRNA co-transfection, and cells were harvested after another 72 h of culture.
556 Sequences of siRNAs are indicated in Table S2.

557

558 **Production of anti-Daed monoclonal antibody**

559 GST-Daed (Met1–Asp197) was expressed in *E. coli* (Rosetta-DE3) and the inclusion
560 bodies were used for mouse immunization. Production and selection of hybridomas that
561 produce anti-Daed monoclonal antibodies were performed as described previously.[79]

562

563 **Mitochondrial fractionation**

564 Mitochondria were fractionated as previously reported.[12] Briefly, 1.2 × 10^8 OSCs were

565 suspended in 500 μL of buffer A [30 mM Tris-HCl (pH 7.3), 225 mM D-mannitol, 75 mM
566 sucrose, and 0.05 mM EGTA] and the cell suspension was passed 30 times through a
567 30-gauge needle attached to a 1-mL syringe. The lysates were centrifuged at 600 *g* for
568 5 min and the supernatants were collected, and repeated twice. The lysates were then
569 centrifuged at 7,000 *g* for 10 min and the supernatants were collected as the cytoplasmic
570 fraction. This step was also repeated twice. The pellets were resuspended in 500 μL of
571 buffer B [30 mM Tris-HCl (pH 7.3), 225 mM D-mannitol, and 75 mM sucrose] and
572 centrifuged at 10,000 *g* for 10 min. The supernatant was used as the mitochondrial
573 fraction.
574
575 **Nuclear fractionation**
576 Nuclear fractionation was performed as previously reported[24] with some modifications.
577 In brief, cells were suspended in hypotonic buffer [10 mM HEPES-KOH (pH 7.3), 10 mM
578 KCl, 1.5 mM $MgCl_2$, 0.5 mM dithiothreitol (DTT), 2 μg/mL leupeptin, 2 μg/mL pepstatin
579 A, and 0.5% aprotinin] by pipetting six times and passed 3 times through a 25-gauge
580 needle attached to a 1-mL syringe. The lysates were centrifuged at 400 *g* for 10 min to
581 collect nuclei. The supernatants were collected as the cytoplasmic fraction, then the
582 concentration of KCl was adjusted to 200 mM and centrifuged at 20,000 *g* for 20 min
583 before used for Piwi-piRISC isolation (see below). The nuclear fraction was washed with
584 hypotonic buffer and resuspended in chromatin co-immunoprecipitation buffer [50 mM
585 HEPES-KOH (pH 7.3), 200 mM KCl, 1 mM EDTA, 1% Triton X-100, 0.1% Na
586 deoxycholate, 2 μg/mL leupeptin, 2 μg/mL pepstatin A, and 0.5% aprotinin]. The nuclear
587 fraction was sonicated and centrifuged at 20,000 *g* for 20 min. The supernatant was
588 collected as nuclear extract fraction for Piwi-piRISC isolation.

589

590 **Western blotting**

591 Western blotting was performed essentially as described previously.[80] Proteins
592 separated on SDS polyacrylamide gels were transferred to ClearTrans SP PVDF
593 membranes (Fujifilm Wako Pure Chemical) and incubated in PBS containing 0.1%
594 Tween-20 (T-PBS) supplemented with 5% skimmed milk. After washing with T-PBS, the
595 membranes were incubated with the following primary antibodies: anti-Daed (1:1,000
596 dilution, this study), anti-Gasz (1:1,000 dilution),[12] anti-Armi (2F8A9, 1:1,000 dilution),[16]
597 anti-Piwi (3G11, 1:1,000 dilution),[35] anti-β-Tub (1:1,000 dilution, E7, Developmental
598 Studies Hybridoma Bank), anti-HSP60(1:500 dilution, LK1, StressMarq Biosciences),
599 anti-Flag M2 (1:5,000 dilution, F3165, Sigma), anti-Histon H3 (1:5,000 dilution, ab1791,
600 abcam) monoclonal and anti-c-Myc (1:1,000 dilution, C3956, Sigma) polycronal
601 antibodies. After washing with T-PBS, the membranes were incubated with peroxidase-
602 conjugated anti-mouse IgG antibodies (1:5,000 dilution, 55558, Cappel) or anti-rabbit
603 IgG antibodies (1:5,000 dilution, 7074, Cell Signaling Technology). The membranes
604 were then reacted with Clarity Western ECL Substrate (Bio-Rad) and images were
605 collected using ChemiDoc XRS Plus System (Bio-Rad). The signal intensity was
606 quantified by Fiji (Ver. 2.0.0-rc-69/1.52p).[70]

607

608 **Immunofluorescence**

609 Immunofluorescence was performed as described previously.[16] OSCs were fixed with
610 4% formaldehyde in PBS. The cells were permeabilized with PBS containing 0.1% Triton
611 X-100, blocked with PBS containing 3% BSA, and incubated with the following primary
612 antibodies: anti-Armi (2F8A9, 1:200 dilution),[16] anti-Piwi (4D2, 1:200 dilution,[35] anti-Yb

613 (1G2H3, 1:200 dilution),[55] anti-Flag M2 (F3165, 1:1,000 dilution, Sigma) monoclonal and
614 anti-c-Myc (1:300 dilution, C3956, Sigma) polyclonal antibodies. Anti-Flag polyclonal
615 antibodies (F7425, 1:300 dilution, Sigma) were used to obtain the results shown in Fig.
616 2F. After washing with PBS, cells were incubated with the following secondary antibodies
617 (1:1,000 dilution): Alexa 488-conjugated anti-mouse IgG1, Alexa 488-conjugated anti-
618 mouse IgG2b, Alexa 555-conjugated anti-mouse IgG1, Alexa 555-conjugated anti-
619 mouse IgG2b, and Alexa 633-conjugated anti-rabbit IgG (all from Thermo Fisher
620 Scientific). Mitochondria were stained with MitoTracker Orange CMXRos (Thermo Fisher
621 Scientific) before fixation. Cells were mounted with VECTASHIELD Mounting Medium
622 with DAPI (Vector Laboratories). Images were obtained using LSM980 laser scanning
623 confocal microscope (Carl Zeiss).
624
625 **Immunoprecipitation**
626 Immunoprecipitation was performed as described previously.[16] Cells were suspended in
627 binding buffer A [30 mM HEPES-KOH (pH 7.3), 150 mM KOAc, 5 mM $Mg(OAc)_2$, 5 mM
628 DTT, 1% Triton X-100, 2 μg/mL leupeptin, 2 μg/mL pepstatin A, and 0.5% aprotinin]
629 supplemented with 0.04 U/μL RNasin Plus RNase Inhibitor (Promega) and the cell
630 suspension was passed 10 times through a 30-gauge needle and centrifuged. The
631 obtained supernatants (cell lysates) were incubated at 4°C with Dynabeads Protein G
632 (Thermo Fisher Scientific) pre-bound with antibodies. After 1 h of incubation, the beads
633 were washed with binding buffer and the materials bound on the beads were analyzed.
634
635 **Piwi-piRISC isolation from OSCs**
636 Cells were lysed by sonication in binding buffer B [50 mM HEPES-KOH (pH 7.3), 200

637 mM KCl, 1 mM EDTA, 1 mM DTT, 1% Triton X-100, 0.1% Na deoxycholate, 2 μg/mL
638 leupeptin, 2 μg/mL pepstatin A, and 0.5% aprotinin] supplemented with 0.1 U/μL RNasin
639 Plus RNase Inhibitor. Cell lysates were then incubated with anti-Piwi monoclonal
640 antibodies (3G11) pre-bound to Dynabeads Protein G at 4°C for 2 h. The beads were
641 washed with IP-wash buffer [20 mM HEPES-KOH (pH 7.3), 300 mM NaCl, 1 mM DTT,
642 0.05% NP-40, 2 μg/mL leupeptin, 2 μg/mL pepstatin A, and 0.5% aprotinin] and with
643 high-salt IP-wash buffer [20 mM HEPES-KOH (pH 7.3), 500 mM NaCl, 1 mM DTT, 0.05%
644 NP-40, 2 μg/mL leupeptin, 2 μg/mL pepstatin A, and 0.5% aprotinin]. RNAs were eluted
645 from the beads with phenol-chloroform and precipitated with ethanol. Eluted RNAs were
646 separated on denaturing polyacrylamide gels and detected by SYBR Gold Nucleic Acid
647 Gel Stain (Thermo Fisher Scientific). Signal intensity was calculated using Fiji, and
648 displayed using Python3 and seaborn[75] (Ver.0.12.2). For piRNA sequencing, cells were
649 lysed in binding buffer C [20 mM HEPES-KOH (pH 7.3), 150 mM NaCl, 1mM EDTA, 1
650 mM DTT, 0.5% NP-40, 2 μg/mL leupeptin, 2 μg/mL pepstatin A, and 0.5% aprotinin]
651 supplemented with 0.04 U/μL RNasin Plus RNase Inhibitor. RNAs were separated on
652 denaturing polyacrylamide gels and 20–40-nt RNAs were eluted from the gels and
653 cloned as described previously.[8] QIAseq FastSelect-rRNA Fly Kit (QIAGEN) was used
654 to remove rRNA from the library.
655
656 **Northern blotting**
657 Total RNAs were isolated from OSCs using ISOGEN II (Fujifilm Wako Pure Chemical)
658 and treated with 0.04 U/μL TURBO DNase (Life Technologies). Northern blotting was
659 carried out as described previously.[81] Total RNAs were separated on denaturing
660 polyacrylamide gels, blotted on Hybond-N+ hybridization membranes (Cytiva), and UV

661 cross-linked. The membranes were incubated at 42°C for 30 min in hybridization buffer
662 [200 mM sodium phosphate buffer (pH 7.2), 7% SDS, and 1 mM EDTA] and probed with
663 ^{32}P-labeled oligonucleotides at 42°C overnight. The membranes were washed with NB-
664 wash buffer [30 mM sodium citrate (pH 7.0), 300 mM NaCl, and 0.1% SDS] at 42°C and
665 scanned using Typhoon FLA 9500 (Cytiva). Sequences of oligodeoxynucleotides are
666 shown in Table S3.
667
668 **RT-qPCR**
669 Total RNAs from OSCs were reverse-transcribed using ReverTra Ace (Toyobo).
670 Resulting cDNAs were amplified with StepOnePlus (Thermo Fisher Scientific) using
671 PowerUp SYBR Green Master Mix (Thermo Fisher Scientific). Sequences of primers are
672 shown in Table S4.
673
674 **Recombinant proteins**
675 GST-Daed ΔTM-His was expressed in *E. coli* (Rosetta DE3) at 16°C overnight. *E. coli*
676 was harvested and lysed by sonication in lysis buffer [30 mM Tris-HCl (pH 8.0), 500 mM
677 NaCl, 1% Triton X-100, 10 mM imidazole, 1× cOmplete ULTRA Tablets (Roche), and 1
678 mM DTT]. The supernatants after centrifugation were bound to Ni-Sepharose 6 Fast
679 Flow (Cytiva) at 4°C for 1 h. After washing with wash buffer A [30 mM Tris-HCl (pH 8.0),
680 500 mM NaCl, 1% Triton X-100, 10 mM imidazole, and 1 mM DTT], proteins were eluted
681 from the beads with elution buffer A [30 mM Tris-HCl (pH 8.0), 150 mM NaCl, 1% Triton
682 X-100, 250 mM imidazole, and 1 mM DTT]. Eluted proteins were bound to Glutathione
683 Sepharose 4B (Cytiva) at 4°C for 1 h. After washing with wash buffer B [30 mM Tris-HCl
684 (pH 8.0), 500 mM NaCl, 1% Triton X-100, and 1 mM DTT], proteins were eluted from the

685 beads with elution buffer B [30 mM Tris-HCl (pH 8.0), 150 mM NaCl, 1% Triton X-100, 1
686 mM DTT, and 15 mM glutathione], dialyzed in dialysis buffer [30 mM Tris-HCl (pH 8.0),
687 150 mM NaCl, 1 mM DTT, 10% glycerol, and 8 μg/mL GST-HRV3C protease], and
688 passed through Glutathione Sepharose 4B to remove the protease and GST.
689
690 **Pull-down assay**
691 OSCs expressing Armi WT-Flag and its ΔN34 mutant were suspended with bait-
692 preparing buffer [30 mM HEPES-KOH (pH 7.3), 150 mM KOAc, 500 mM NaCl, 5 mM
693 $Mg(OAc)_2$, 5 mM DTT, 1% Triton X-100, 2 μg/mL leupeptin, 2 μg/mL pepstatin A, 0.5%
694 aprotinin, and 25 μg/mL RNase A (Roche)]. The cell suspension was passed five times
695 through a 25-gauge needle and another five times through a 30-gauge needle, and then
696 centrifuged. The supernatants were incubated at 4°C for 1 h with anti-Flag antibodies
697 pre-bound onto Dynabeads Protein G. Beads were washed with bait-preparing buffer
698 and then binding buffer D [30 mM Tris-HCl (pH 8.0), 150 mM NaCl, 1 mM DTT, and 1%
699 Triton X-100]. Daed ΔTM-His was added to the beads and incubated at 4°C for 1.5 h.
700 After washing with binding buffer, proteins were eluted from the beads, separated on an
701 SDS polyacrylamide gel, and stained with CBB.
702
703 **β-elimination assay**
704 β-elimination was performed as described previously with some modifications.[36] piRNAs
705 were isolated from Piwi immunoprecipitated from OSCs. miRNAs were isolated from
706 Ago1 immunoprecipitated from OSCs using monoclonal anti-Ago1 antibodies[56]. RNAs
707 were incubated in 10 mM $NaIO_4$ for 40 min at 0°C in the dark. After ethanol precipitation,
708 RNAs were dissolved in 1 M L(+)-lysine-HCl (pH 8.5) and incubated for 90 min at 45°C.

709 After ethanol precipitation, RNAs were separated on a denaturing polyacrylamide gel
710 and detected by SYBR Gold Nucleic Acid Gel Stain.
711
712 **piRNA sequencing and bioinformatic analysis**
713 piRNAs were sequenced using MiSeq (Illumina) with MiSeq Reagent Kit v3 (Illumina).
714 piRNA-seq analysis was performed as described previously[8] with some modifications.
715 Adapter-trimmed reads of ≥ 18 nt in length were mapped against the *Drosophila* genome
716 (BDGP Release 6 + ISO1 MT/dm6) with FlyBase gene model (Release 6.21) using
717 STAR[63] (Ver. 2.7.8a). Uniquely mapped reads with up to one mismatch were used for
718 the subsequent analysis. Read length of each biological triplicate was used in the
719 analysis in Figs. 4B and S4I. After confirming high correlations between samples (Figure
720 S6A, B), reads were merged and used for subsequent analysis. Reads mapped to exons
721 of coding genes (Figure S6A, B) were counted with HTSeq[64] (Ver. 0.9.1) using
722 annotation file obtained from FlyBase and normalized to RPM+1 reads. Spearman's rho
723 was calculated using R[61] (Ver. 4.3.1). For transposon annotation (Fig. S4B,C), the
724 annotation file of repeat sequences was obtained from RepeatMasker (dm6-Apr 2006-
725 RepeatMasker open-4.0.6-Dfam 2.0) and transposons were extracted without distinction
726 between int and LTR. Reads mapped antisense to transposons were counted using
727 HTSeq. For the analysis in Fig. S4C, reads were normalized to RPM+1 reads. For the
728 analysis in Fig. S4B, transposons which mapped > 5 RPM reads in the sum of WT and
729 ΔSAM were selected, and the mean length of mapped reads for each transposon were
730 calculated. For 1U bias and +1U bias analyses (Figs. 4C, I and S4J), the 5′ ends and
731 their downstream sequences of piRNAs (1U bias) or *Drosophila* genome sequences
732 around the 3′ ends (+1U bias) were obtained using bedtools[65] (Ver. 2.30.0) and SAMtools

733 (Ver. 1.9).[66] Sequence logos were generated using ggseqlogo.[68] For the phasing
734 analysis (Fig. 4D), 3′ end positions around piRNA 5′ end position were normalized to
735 RPM and showed in heatmaps using RSeQC[69] (Ver. 2.6.4), deepTools[67] (Ver. 3.3.2),
736 SAMtools[66] (Ver. 1.9) and "wigToBigWig" from UCSC. Binary histograms were
737 generated using the matrix of heatmaps. Values were transformed into binary format
738 (counts = 0 → 0, counts > 0 → 1) in accordance with a previous study.[18] For the
739 comparison of 3′ end position in WT and mutant libraries of Daed or Armi (Figs. 4H and
740 S4K), 50,000 piRNA 5′ end positions, common to the WT and mutant libraries and most
741 abundant in the WT library, were extracted. The percentage of 3′ end positions
742 corresponding to each 5′ end position was calculated and shown in heatmaps. 5′ end
743 positions were ordered by the 3′ end position of WT library data and the same order was
744 maintained in the mutant library data. To obtain the results shown in Fig. S4G, 5′-end
745 positions that dominantly produce 26- or 27-nt piRNAs in the WT library were extracted,
746 and after combining, these piRNAs were classified as "Unchanged" (51,833 positions)
747 and "Elongated" (53,258 positions) according to 3′-end elongation caused by Daed SAM
748 loss and used for further analysis.
749
750 **piRISC production simulation**
751 The *flam* sequence was downloaded from FlyBase (Release FB2023_05) (21,629,891
752 to 21,792,731 on the X chromosome) and subjected to the digestion into 163 piRNA
753 precursors (starting at U and around 1,000 nt). The precursors were cleaved to 18–40-
754 nt piRNAs immediately before U. The cleavage position was determined based on the
755 distribution of the actual piRNA length, which was obtained by fitting a normal distribution
756 to the piRNA sequencing data. The simulation was performed using Python3[57] (Ver.

757 3.8.8) with add-on libraries [Numpy[58] (Ver. 1.20.1), Scipy[59] (Ver. 1.6.2), and Pandas[60]
758 (Ver. 1.2.4)].
759
760 **Structure prediction**
761 A structure model of the AmTEC (Fig. 1A) and Armi–AmTEC complex (Fig. 3A) was built
762 by structure prediction with ColabFold[82] (Ver. 1.5.5) and AlphaFold[31] (Ver. 2.3) using
763 protein amino acid sequences from FlyBase (Release FB2023_04). Five complex
764 models were built, and structural predictions and optimization were performed five times
765 for each complex model. The structure model with the highest pLDDT value underwent
766 relax steps. The N-terminal disorder region and TM domain orientations of Daed and
767 Gasz were appropriately changed at the linker region using ISOLDE[72] (Ver. 1.6). The
768 structure was visualized using UCSF ChimeraX[71] (Ver. 1.6.1).
769
770 **Ortholog search and protein sequence alignment**
771 Orthologs for Armi/MOV10L1, Gasz/ASZ1, PNLDC1, Papi/TDRKH, Nbr were searched
772 using OrthoDB v11. Orthologs for Daed were searched using OrthoDB v11[38] and NCBI
773 PSI-Blast. Species taxonomy was according to NCBI and phylogenetic tree (Figure 5A)
774 were generated following previous studies.[84,85] Multiple sequence alignment (Figure
775 S5B) was conducted using CLUSTAL Omega multiple alignment[73] and visualized using
776 ESPript (Ver. 3.0).[76] The phylogenetic tree (Figure 5SA) was generated using Neighbor-
777 Joining method[83] in MEGA11[77]. Multiple sequence alignment (Figure S5C) was
778 conducted using CLUSTAL Omega multiple alignment[73] and visualized using iTOL (Ver.
779 6.9).[74] The following protein sequences were acquired from NCBI: *D. melanogaster* Armi
780 (NP_001014556), *H. sapiens* Moloney leukemia virus 10-like protein 1 (MOV10L1)

781 (NP_061868.1), *M. musculus* MOV10L1 (XP_006521619.1), *G. gallus* MOV10L1
782 (XP_040514825.1), *X. tropicalis* MOV10L1 (NP_001072624.1), *D. rerio* MOV10L1
783 (NP_001070795.1), *Z. nevadensis* Armi (XP_021937793.1), *T. palmi* Armi
784 (XP_034251738.1), *A. echinatior* Armi (XP_011062616.1), *B. terrestris* Armi
785 (XP_012166280.1), *D. ponderosae* Armi (XP_048525683.1), *T. castaneum* Armi
786 (XP_008199251.1), *B. anynana* Armi (XP_023946786.2), *B. mori* Armi
787 (XP_037867032.1), *A. gambiae* Armi (XP_061506580.1), *A. aegypti* Armi
788 (XP_021698921.1), *B. dorsalis* Armi (XP_011214121.1), *C. capitata* Armi
789 (XP_004537921.1), *M. domestica* Armi (XP_058975516.1) and *S. calcitrans* Armi
790 (XP_013110641.2).
791
792 **Quantification and statistical analysis**
793 All experiments were performed over two independent experiments (biological
794 replicates). Sample sizes were predetermined following previously performed
795 experiments with similar setup in the field. Statistical methods, *p* value and number of
796 replicates are indicated in each figure and its legend. Statistical analyses were performed
797 in the R software environment (version 4.3.1). Shapiro-Wilk test was used for testing
798 normality when statistical methods based on the normal distribution was used.
799 Experiments were not blinded as consistent with the previous studies in the field.
800
801 **Supplemental figure titles**
802 Figure S1. Related to Figure1; Coiled-coil prediction and specificity of anti-Daed
803 antibodies
804 Figure S2. Related to Figure2; Functions and behaviors of Daed and Gasz in OSCs

805 Figure S3. Related to Figure3; Effects of Armi mutants on piRNA biogenesis and Piwi-
806 piRISC function
807 Figure S4. Related to Figure4; Effects of Daed and Armi mutants on piRNA biogenesis
808 and Piwi-piRISC function
809 Figure S5. Related to Figure5; Sequence alignment of Daed and Armi UPF1-like domain
810 in species
811 Figure S6. Related to STAR Method "piRNA sequencing and bioinformatic analysis";
812 Reproducibility of piRNA-seq
813
814 **Supplemental table titles**
815 Table S1. Related to STAR Method "Plasmid construction"; Sequences of primers used
816 for plasmid construction
817 Table S2. Related to STAR Method "RNAi and transfection"; Sequences of siRNAs
818 Table S3. Related to STAR Method "Northern blotting"; Sequences of oligos used for
819 northern blotting
820 Table S4. Related to STAR Method "RT-qPCR"; Sequences of primers used for RT-
821 qPCR
822
823 **References**
824 1. Czech, B., Munafò, M., Ciabrelli, F., Eastwood, E.L., Fabry, M.H., Kneuss, E., and
825 Hannon, G.J. (2018). piRNA-Guided Genome Defense: From Biogenesis to
826 Silencing. Annual Review of Genetics *52*, 131–157.
827 https://doi.org/10.1146/annurev-genet-120417-031441.
828 2. Huang, X., Fejes Tóth, K., and Aravin, A.A. (2017). piRNA Biogenesis in
829 Drosophila melanogaster. Trends in Genetics *33*, 882–894.
830 https://doi.org/10.1016/j.tig.2017.09.002.
831 3. Ozata, D.M., Gainetdinov, I., Zoch, A., O'Carroll, D., and Zamore, P.D. (2019).

832 PIWI-interacting RNAs: small RNAs with big functions. Nat Rev Genet *20*, 89–108.
833 https://doi.org/10.1038/s41576-018-0073-3.
834 4. Yamashiro, H., and Siomi, M.C. (2018). PIWI-Interacting RNA in Drosophila:
835 Biogenesis, Transposon Regulation, and Beyond. Chem Rev *118*, 4404–4421.
836 https://doi.org/10.1021/acs.chemrev.7b00393.
837 5. Brennecke, J., Aravin, A.A., Stark, A., Dus, M., Kellis, M., Sachidanandam, R., and
838 Hannon, G.J. (2007). Discrete Small RNA-Generating Loci as Master Regulators
839 of Transposon Activity in Drosophila. Cell *128*, 1089–1103.
840 https://doi.org/10.1016/j.cell.2007.01.043.
841 6. Malone, C.D., Brennecke, J., Dus, M., Stark, A., McCombie, W.R.,
842 Sachidanandam, R., and Hannon, G.J. (2009). Specialized piRNA Pathways Act in
843 Germline and Somatic Tissues of the Drosophila Ovary. Cell *137*, 522–535.
844 https://doi.org/10.1016/j.cell.2009.03.040.
845 7. Goriaux, C., Desset, S., Renaud, Y., Vaury, C., and Brasset, E. (2014).
846 Transcriptional properties and splicing of the flamenco piRNA cluster. EMBO
847 reports *15*, 411–418. https://doi.org/10.1002/embr.201337898.
848 8. Hirakata, S., Ishizu, H., Fujita, A., Tomoe, Y., and Siomi, M.C. (2019).
849 Requirements for multivalent Yb body assembly in transposon silencing in
850 Drosophila. EMBO Rep *20*, e47708. https://doi.org/10.15252/embr.201947708.
851 9. Ishizu, H., Iwasaki, Y.W., Hirakata, S., Ozaki, H., Iwasaki, W., Siomi, H., and
852 Siomi, M.C. (2015). Somatic Primary piRNA Biogenesis Driven by cis-Acting RNA
853 Elements and trans-Acting Yb. Cell Reports *12*, 429–440.
854 https://doi.org/10.1016/j.celrep.2015.06.035.
855 10. Cora, E., Pandey, R.R., Xiol, J., Taylor, J., Sachidanandam, R., McCarthy, A.A.,
856 and Pillai, R.S. (2014). The MID-PIWI module of Piwi proteins specifies nucleotide-
857 and strand-biases of piRNAs. RNA *20*, 773–781.
858 https://doi.org/10.1261/rna.044701.114.
859 11. Stein, C.B., Genzor, P., Mitra, S., Elchert, A.R., Ipsaro, J.J., Benner, L., Sobti, S.,
860 Su, Y., Hammell, M., Joshua-Tor, L., et al. (2019). Decoding the 5′ nucleotide bias
861 of PIWI-interacting RNAs. Nat Commun *10*, 828. https://doi.org/10.1038/s41467-
862 019-08803-z.
863 12. Yamashiro, H., Negishi, M., Kinoshita, T., Ishizu, H., Ohtani, H., and Siomi, M.C.
864 (2020). Armitage determines Piwi–piRISC processing from precursor formation
865 and quality control to inter-organelle translocation. EMBO reports *21*, e48769.
866 https://doi.org/10.15252/embr.201948769.
867 13. Choi, S.-Y., Huang, P., Jenkins, G.M., Chan, D.C., Schiller, J., and Frohman, M.A.

868 (2006). A common lipid links Mfn-mediated mitochondrial fusion and SNARE-
869 regulated exocytosis. Nat Cell Biol *8*, 1255–1262. https://doi.org/10.1038/ncb1487.
870 14. Ipsaro, J.J., Haase, A.D., Knott, S.R., Joshua-Tor, L., and Hannon, G.J. (2012).
871 The structural biochemistry of Zucchini implicates it as a nuclease in piRNA
872 biogenesis. Nature *491*, 279–283. https://doi.org/10.1038/nature11502.
873 15. Nishimasu, H., Ishizu, H., Saito, K., Fukuhara, S., Kamatani, M.K., Bonnefond, L.,
874 Matsumoto, N., Nishizawa, T., Nakanaga, K., Aoki, J., et al. (2012). Structure and
875 function of Zucchini endoribonuclease in piRNA biogenesis. Nature *491*, 284–287.
876 https://doi.org/10.1038/nature11509.
877 16. Saito, K., Ishizu, H., Komai, M., Kotani, H., Kawamura, Y., Nishida, K.M., Siomi,
878 H., and Siomi, M.C. (2010). Roles for the Yb body components Armitage and Yb in
879 primary piRNA biogenesis in Drosophila. Genes Dev *24*, 2493–2498.
880 https://doi.org/10.1101/gad.1989510.
881 17. Han, B.W., Wang, W., Li, C., Weng, Z., and Zamore, P.D. (2015). Noncoding RNA.
882 piRNA-guided transposon cleavage initiates Zucchini-dependent, phased piRNA
883 production. Science *348*, 817–821. https://doi.org/10.1126/science.aaa1264.
884 18. Mohn, F., Handler, D., and Brennecke, J. (2015). piRNA-guided slicing specifies
885 transcripts for Zucchini-dependent, phased piRNA biogenesis. Science *348*, 812–
886 817. https://doi.org/10.1126/science.aaa1039.
887 19. Yashiro, R., Murota, Y., Nishida, K.M., Yamashiro, H., Fujii, K., Ogai, A.,
888 Yamanaka, S., Negishi, L., Siomi, H., and Siomi, M.C. (2018). Piwi Nuclear
889 Localization and Its Regulatory Mechanism in Drosophila Ovarian Somatic Cells.
890 Cell Reports *23*, 3647–3657. https://doi.org/10.1016/j.celrep.2018.05.051.
891 20. Dönertas, D., Sienski, G., and Brennecke, J. (2013). Drosophila Gtsf1 is an
892 essential component of the Piwi-mediated transcriptional silencing complex. Genes
893 Dev *27*, 1693–1705. https://doi.org/10.1101/gad.221150.113.
894 21. Fabry, M.H., Ciabrelli, F., Munafò, M., Eastwood, E.L., Kneuss, E., Falciatori, I.,
895 Falconio, F.A., Hannon, G.J., and Czech, B. (2019). piRNA-guided co-
896 transcriptional silencing coopts nuclear export factors. eLife *8*, e47999.
897 https://doi.org/10.7554/eLife.47999.
898 22. Murano, K., Iwasaki, Y.W., Ishizu, H., Mashiko, A., Shibuya, A., Kondo, S., Adachi,
899 S., Suzuki, S., Saito, K., Natsume, T., et al. (2019). Nuclear RNA export factor
900 variant initiates piRNA-guided co-transcriptional silencing. The EMBO Journal *38*,
901 e102870. https://doi.org/10.15252/embj.2019102870.
902 23. Ohtani, H., Iwasaki, Y.W., Shibuya, A., Siomi, H., Siomi, M.C., and Saito, K.
903 (2013). DmGTSF1 is necessary for Piwi–piRISC-mediated transcriptional

904 transposon silencing in the Drosophila ovary. Genes Dev *27*, 1656–1661.
905 https://doi.org/10.1101/gad.221515.113.
906 24. Onishi, R., Sato, K., Murano, K., Negishi, L., Siomi, H., and Siomi, M.C. (2020).
907 Piwi suppresses transcription of Brahma-dependent transposons via Maelstrom in
908 ovarian somatic cells. Science Advances *6*, eaaz7420.
909 https://doi.org/10.1126/sciadv.aaz7420.
910 25. Sienski, G., Dönertas, D., and Brennecke, J. (2012). Transcriptional silencing of
911 transposons by Piwi and maelstrom and its impact on chromatin state and gene
912 expression. Cell *151*, 964–980. https://doi.org/10.1016/j.cell.2012.10.040.
913 26. Sienski, G., Batki, J., Senti, K.-A., Dönertas, D., Tirian, L., Meixner, K., and
914 Brennecke, J. (2015). Silencio/CG9754 connects the Piwi–piRNA complex to the
915 cellular heterochromatin machinery. Genes Dev *29*, 2258–2271.
916 https://doi.org/10.1101/gad.271908.115.
917 27. Yu, Y., Gu, J., Jin, Y., Luo, Y., Preall, J.B., Ma, J., Czech, B., and Hannon, G.J.
918 (2015). Panoramix enforces piRNA-dependent cotranscriptional silencing. Science
919 *350*, 339–342. https://doi.org/10.1126/science.aab0700.
920 28. Czech, B., Preall, J.B., McGinn, J., and Hannon, G.J. (2013). A transcriptome-wide
921 RNAi screen in the Drosophila ovary reveals factors of the germline piRNA
922 pathway. Mol Cell *50*, 749–761. https://doi.org/10.1016/j.molcel.2013.04.007.
923 29. Munafò, M., Manelli, V., Falconio, F.A., Sawle, A., Kneuss, E., Eastwood, E.L.,
924 Seah, J.W.E., Czech, B., and Hannon, G.J. (2019). Daedalus and Gasz recruit
925 Armitage to mitochondria, bringing piRNA precursors to the biogenesis machinery.
926 Genes Dev. *33*, 844–856. https://doi.org/10.1101/gad.325662.119.
927 30. Evans, R., O'Neill, M., Pritzel, A., Antropova, N., Senior, A., Green, T., Žídek, A.,
928 Bates, R., Blackwell, S., Yim, J., et al. (2022). Protein complex prediction with
929 AlphaFold-Multimer. Preprint at bioRxiv,
930 https://doi.org/10.1101/2021.10.04.463034
931 https://doi.org/10.1101/2021.10.04.463034.
932 31. Jumper, J., Evans, R., Pritzel, A., Green, T., Figurnov, M., Ronneberger, O.,
933 Tunyasuvunakool, K., Bates, R., Žídek, A., Potapenko, A., et al. (2021). Highly
934 accurate protein structure prediction with AlphaFold. Nature *596*, 583–589.
935 https://doi.org/10.1038/s41586-021-03819-2.
936 32. Madeo, G., Savojardo, C., Manfredi, M., Martelli, P.L., and Casadio, R. (2023).
937 CoCoNat: a novel method based on deep learning for coiled-coil prediction.
938 Bioinformatics *39*, btad495. https://doi.org/10.1093/bioinformatics/btad495.
939 33. Saito, K., Inagaki, S., Mituyama, T., Kawamura, Y., Ono, Y., Sakota, E., Kotani, H.,

Asai, K., Siomi, H., and Siomi, M.C. (2009). A regulatory circuit for piwi by the large Maf gene traffic jam in Drosophila. Nature *461*, 1296–1299. https://doi.org/10.1038/nature08501.

34. Olivieri, D., Sykora, M.M., Sachidanandam, R., Mechtler, K., and Brennecke, J. (2010). An in vivo RNAi assay identifies major genetic and cellular requirements for primary piRNA biogenesis in Drosophila. EMBO J *29*, 3301–3317. https://doi.org/10.1038/emboj.2010.212.
35. Saito, K., Nishida, K.M., Mori, T., Kawamura, Y., Miyoshi, K., Nagami, T., Siomi, H., and Siomi, M.C. (2006). Specific association of Piwi with rasiRNAs derived from retrotransposon and heterochromatic regions in the Drosophila genome. Genes Dev *20*, 2214–2222. https://doi.org/10.1101/gad.1454806.
36. Gunawardane, L.S., Saito, K., Nishida, K.M., Miyoshi, K., Kawamura, Y., Nagami, T., Siomi, H., and Siomi, M.C. (2007). A Slicer-Mediated Mechanism for Repeat-Associated siRNA 5' End Formation in Drosophila. Science *315*, 1587–1590. https://doi.org/10.1126/science.1140494.
37. Horwich, M.D., Li, C., Matranga, C., Vagin, V., Farley, G., Wang, P., and Zamore, P.D. (2007). The Drosophila RNA Methyltransferase, DmHen1, Modifies Germline piRNAs and Single-Stranded siRNAs in RISC. Current Biology *17*, 1265–1272. https://doi.org/10.1016/j.cub.2007.06.030.
38. Kuznetsov, D., Tegenfeldt, F., Manni, M., Seppey, M., Berkeley, M., Kriventseva, E.V., and Zdobnov, E.M. (2023). OrthoDB v11: annotation of orthologs in the widest sampling of organismal diversity. Nucleic Acids Research *51*, D445–D451. https://doi.org/10.1093/nar/gkac998.
39. Vourekas, A., Zheng, K., Fu, Q., Maragkakis, M., Alexiou, P., Ma, J., Pillai, R.S., Mourelatos, Z., and Wang, P.J. (2015). The RNA helicase MOV10L1 binds piRNA precursors to initiate piRNA processing. Genes Dev *29*, 617–629. https://doi.org/10.1101/gad.254631.114.
40. Zheng, K., Xiol, J., Reuter, M., Eckardt, S., Leu, N.A., McLaughlin, K.J., Stark, A., Sachidanandam, R., Pillai, R.S., and Wang, P.J. (2010). Mouse MOV10L1 associates with Piwi proteins and is an essential component of the Piwi-interacting RNA (piRNA) pathway. Proceedings of the National Academy of Sciences *107*, 11841–11846. https://doi.org/10.1073/pnas.1003953107.
41. Ikeda, S., Tanaka, K., Ohtani, R., Kanda, A., Sotomaru, Y., Kono, T., and Obata, Y. (2022). Disruption of piRNA machinery by deletion of ASZ1/GASZ results in the expression of aberrant chimeric transcripts in gonocytes. Journal of Reproduction and Development *68*, 125–136. https://doi.org/10.1262/jrd.2021-146.

42. Ding, D., Liu, J., Dong, K., Midic, U., Hess, R.A., Xie, H., Demireva, E.Y., and Chen, C. (2017). PNLDC1 is essential for piRNA 3′ end trimming and transposon silencing during spermatogenesis in mice. Nat Commun *8*, 819. https://doi.org/10.1038/s41467-017-00854-4.
43. Nishimura, T., Nagamori, I., Nakatani, T., Izumi, N., Tomari, Y., Kuramochi-Miyagawa, S., and Nakano, T. (2018). PNLDC1, mouse pre-piRNA Trimmer, is required for meiotic and post-meiotic male germ cell development. EMBO reports *19*, e44957. https://doi.org/10.15252/embr.201744957.
44. Hayashi, R., Schnabl, J., Handler, D., Mohn, F., Ameres, S.L., and Brennecke, J. (2016). Genetic and mechanistic diversity of piRNA 3' end formation. Nature *539*, 588–592. https://doi.org/10.1038/nature20162.
45. Honda, S., Kirino, Y., Maragkakis, M., Alexiou, P., Ohtaki, A., Murali, R., Mourelatos, Z., and Kirino, Y. (2013). Mitochondrial protein BmPAPI modulates the length of mature piRNAs. RNA *19*, 1405–1418. https://doi.org/10.1261/rna.040428.113.
46. Saxe, J.P., Chen, M., Zhao, H., and Lin, H. (2013). Tdrkh is essential for spermatogenesis and participates in primary piRNA biogenesis in the germline. The EMBO Journal *32*, 1869–1885. https://doi.org/10.1038/emboj.2013.121.
47. Feltzin, V.L., Khaladkar, M., Abe, M., Parisi, M., Hendriks, G.-J., Kim, J., and Bonini, N.M. (2015). The exonuclease Nibbler regulates age-associated traits and modulates piRNA length in Drosophila. Aging Cell *14*, 443–452. https://doi.org/10.1111/acel.12323.
48. Joosten, J., Overheul, G.J., Van Rij, R.P., and Miesen, P. (2021). Endogenous piRNA-guided slicing triggers responder and trailer piRNA production from viral RNA in Aedes aegypti mosquitoes. Nucleic Acids Research *49*, 8886–8899. https://doi.org/10.1093/nar/gkab640.
49. Wang, H., Ma, Z., Niu, K., Xiao, Y., Wu, X., Pan, C., Zhao, Y., Wang, K., Zhang, Y., and Liu, N. (2016). Antagonistic roles of Nibbler and Hen1 in modulating piRNA 3′ ends in Drosophila. Development *143*, 530–539. https://doi.org/10.1242/dev.128116.
50. Ishizu, H., Kinoshita, T., Hirakata, S., Komatsuzaki, C., and Siomi, M.C. (2019). Distinct and Collaborative Functions of Yb and Armitage in Transposon-Targeting piRNA Biogenesis. Cell Reports *27*, 1822-1835.e8. https://doi.org/10.1016/j.celrep.2019.04.029.
51. Lee, Y.C.G., and Langley, C.H. (2012). Long-Term and Short-Term Evolutionary Impacts of Transposable Elements on Drosophila. Genetics *192*, 1411–1432.

https://doi.org/10.1534/genetics.112.145714.
52. Obbard, D.J., Gordon, K.H.J., Buck, A.H., and Jiggins, F.M. (2008). The evolution of RNAi as a defence against viruses and transposable elements. Philosophical Transactions of the Royal Society B: Biological Sciences *364*, 99–115. https://doi.org/10.1098/rstb.2008.0168.
53. Parhad, S.S., and Theurkauf, W.E. (2019). Rapid evolution and conserved function of the piRNA pathway. Open Biology *9*, 180181. https://doi.org/10.1098/rsob.180181.
54. Gamez, S., Srivastav, S., Akbari, O.S., and Lau, N.C. (2020). Diverse Defenses: A Perspective Comparing Dipteran Piwi-piRNA Pathways. Cells *9*, 2180. https://doi.org/10.3390/cells9102180.
55. Murota, Y., Ishizu, H., Nakagawa, S., Iwasaki, Y.W., Shibata, S., Kamatani, M.K., Saito, K., Okano, H., Siomi, H., and Siomi, M.C. (2014). Yb integrates piRNA intermediates and processing factors into perinuclear bodies to enhance piRISC assembly. Cell Rep *8*, 103–113. https://doi.org/10.1016/j.celrep.2014.05.043.
56. Okamura, K., Ishizuka, A., Siomi, H., and Siomi, M.C. (2004). Distinct roles for Argonaute proteins in small RNA-directed RNA cleavage pathways. Genes Dev *18*, 1655–1666. https://doi.org/10.1101/gad.1210204.
57. Van Rossum, G., and Drake, F.L. (2009). Python 3 Reference Manual (CreateSpace).
58. Harris, C.R., Millman, K.J., van der Walt, S.J., Gommers, R., Virtanen, P., Cournapeau, D., Wieser, E., Taylor, J., Berg, S., Smith, N.J., et al. (2020). Array programming with NumPy. Nature *585*, 357–362. https://doi.org/10.1038/s41586-020-2649-2.
59. Virtanen, P., Gommers, R., Oliphant, T.E., Haberland, M., Reddy, T., Cournapeau, D., Burovski, E., Peterson, P., Weckesser, W., Bright, J., et al. (2020). SciPy 1.0: fundamental algorithms for scientific computing in Python. Nat Methods *17*, 261–272. https://doi.org/10.1038/s41592-019-0686-2.
60. McKinney, W. (2010). Data Structures for Statistical Computing in Python. Proceedings of the 9th Python in Science Conference, 56–61. https://doi.org/10.25080/Majora-92bf1922-00a.
61. R Development Core Team (2023). R : A language and environment for statistical computing. R Foundation for Statistical Computing, Vienna, Austria.
62. Martin, M. (2011). Cutadapt removes adapter sequences from high-throughput sequencing reads. EMBnet.journal *17*, 10–12. https://doi.org/10.14806/ej.17.1.200.
63. Dobin, A., Davis, C.A., Schlesinger, F., Drenkow, J., Zaleski, C., Jha, S., Batut, P.,

1048 Chaisson, M., and Gingeras, T.R. (2013). STAR: ultrafast universal RNA-seq
1049 aligner. Bioinformatics *29*, 15–21. https://doi.org/10.1093/bioinformatics/bts635.
1050 64. Anders, S., Pyl, P.T., and Huber, W. (2015). HTSeq--a Python framework to work
1051 with high-throughput sequencing data. Bioinformatics *31*, 166–169.
1052 https://doi.org/10.1093/bioinformatics/btu638.
1053 65. Quinlan, A.R., and Hall, I.M. (2010). BEDTools: a flexible suite of utilities for
1054 comparing genomic features. Bioinformatics *26*, 841–842.
1055 https://doi.org/10.1093/bioinformatics/btq033.
1056 66. Li, H., Handsaker, B., Wysoker, A., Fennell, T., Ruan, J., Homer, N., Marth, G.,
1057 Abecasis, G., Durbin, R., and 1000 Genome Project Data Processing Subgroup
1058 (2009). The Sequence Alignment/Map format and SAMtools. Bioinformatics *25*,
1059 2078–2079. https://doi.org/10.1093/bioinformatics/btp352.
1060 67. Ramírez, F., Ryan, D.P., Grüning, B., Bhardwaj, V., Kilpert, F., Richter, A.S.,
1061 Heyne, S., Dündar, F., and Manke, T. (2016). deepTools2: a next generation web
1062 server for deep-sequencing data analysis. Nucleic Acids Res *44*, W160-165.
1063 https://doi.org/10.1093/nar/gkw257.
1064 68. Wagih, O. (2017). ggseqlogo: a versatile R package for drawing sequence logos.
1065 Bioinformatics *33*, 3645–3647. https://doi.org/10.1093/bioinformatics/btx469.
1066 69. Wang, L., Wang, S., and Li, W. (2012). RSeQC: quality control of RNA-seq
1067 experiments. Bioinformatics *28*, 2184–2185.
1068 https://doi.org/10.1093/bioinformatics/bts356.
1069 70. Schindelin, J., Arganda-Carreras, I., Frise, E., Kaynig, V., Longair, M., Pietzsch, T.,
1070 Preibisch, S., Rueden, C., Saalfeld, S., Schmid, B., et al. (2012). Fiji: an open-
1071 source platform for biological-image analysis. Nat Methods *9*, 676–682.
1072 https://doi.org/10.1038/nmeth.2019.
1073 71. Pettersen, E.F., Goddard, T.D., Huang, C.C., Meng, E.C., Couch, G.S., Croll, T.I.,
1074 Morris, J.H., and Ferrin, T.E. (2021). UCSF ChimeraX: Structure visualization for
1075 researchers, educators, and developers. Protein Science *30*, 70–82.
1076 https://doi.org/10.1002/pro.3943.
1077 72. Croll, T.I. (2018). ISOLDE: a physically realistic environment for model building into
1078 low-resolution electron-density maps. Acta Crystallogr D Struct Biol *74*, 519–530.
1079 https://doi.org/10.1107/S2059798318002425.
1080 73. Madeira, F., Pearce, M., Tivey, A.R.N., Basutkar, P., Lee, J., Edbali, O.,
1081 Madhusoodanan, N., Kolesnikov, A., and Lopez, R. (2022). Search and sequence
1082 analysis tools services from EMBL-EBI in 2022. Nucleic Acids Res *50*, W276–
1083 W279. https://doi.org/10.1093/nar/gkac240.

1084 74. Letunic, I., and Bork, P. (2024). Interactive Tree of Life (iTOL) v6: recent updates
1085 to the phylogenetic tree display and annotation tool. Nucleic Acids Research,
1086 gkae268. https://doi.org/10.1093/nar/gkae268.
1087 75. Waskom, M.L. (2021). seaborn: statistical data visualization. Journal of Open
1088 Source Software *6*, 3021. https://doi.org/10.21105/joss.03021.
1089 76. Robert, X., and Gouet, P. (2014). Deciphering key features in protein structures
1090 with the new ENDscript server. Nucleic Acids Research *42*, W320–W324.
1091 https://doi.org/10.1093/nar/gku316.
1092 77. Tamura, K., Stecher, G., and Kumar, S. (2021). MEGA11: Molecular Evolutionary
1093 Genetics Analysis Version 11. Molecular Biology and Evolution *38*, 3022–3027.
1094 https://doi.org/10.1093/molbev/msab120.
1095 78. Nye, J., Buster, D.W., and Rogers, G.C. (2014). The use of cultured Drosophila
1096 cells for studying the microtubule cytoskeleton. Methods Mol Biol *1136*, 81–101.
1097 https://doi.org/10.1007/978-1-4939-0329-0_6.
1098 79. Nishida, K.M., Iwasaki, Y.W., Murota, Y., Nagao, A., Mannen, T., Kato, Y., Siomi,
1099 H., and Siomi, M.C. (2015). Respective functions of two distinct Siwi complexes
1100 assembled during PIWI-interacting RNA biogenesis in Bombyx germ cells. Cell
1101 Rep *10*, 193–203. https://doi.org/10.1016/j.celrep.2014.12.013.
1102 80. Miyoshi, K., Tsukumo, H., Nagami, T., Siomi, H., and Siomi, M.C. (2005). Slicer
1103 function of Drosophila Argonautes and its involvement in RISC formation. Genes
1104 Dev *19*, 2837–2848. https://doi.org/10.1101/gad.1370605.
1105 81. Saito, K., Ishizuka, A., Siomi, H., and Siomi, M.C. (2005). Processing of pre-
1106 microRNAs by the Dicer-1-Loquacious complex in Drosophila cells. PLoS Biol *3*,
1107 e235. https://doi.org/10.1371/journal.pbio.0030235.
1108 82. Mirdita, M., Schütze, K., Moriwaki, Y., Heo, L., Ovchinnikov, S., and Steinegger, M.
1109 (2022). ColabFold: making protein folding accessible to all. Nat Methods *19*, 679–
1110 682. https://doi.org/10.1038/s41592-022-01488-1.
1111 83. Saitou, N., and Nei, M. (1987). The neighbor-joining method: a new method for
1112 reconstructing phylogenetic trees. Mol Biol Evol *4*, 406–425.
1113 https://doi.org/10.1093/oxfordjournals.molbev.a040454.
1114 84. Lambkin, C.L., Sinclair, B.J., Pape, T., Courtney, G.W., Skevington, J.H., Meier,
1115 R., Yeates, D.K., Blagoderov, V., and Wiegmann, B.M. (2013). The phylogenetic
1116 relationships among infraorders and superfamilies of Diptera based on
1117 morphological evidence. Systematic Entomology *38*, 164–179.
1118 https://doi.org/10.1111/j.1365-3113.2012.00652.x.
1119 85. Misof, B., Liu, S., Meusemann, K., Peters, R.S., Donath, A., Mayer, C., Frandsen,

1120 P.B., Ware, J., Flouri, T., Beutel, R.G., et al. (2014). Phylogenomics resolves the
1121 timing and pattern of insect evolution. Science *346*, 763–767.
1122 https://doi.org/10.1126/science.1257570.

1123

1124 **Supplemental figure legends**

1125 **Figure S1. Coiled-coil prediction and specificity of anti-Daed antibodies**

1126 (**A**) Sequence-based CC prediction of Daed (upper) and Gasz (lower) by CoCoNat.[32]
1127 Red line indicates the CC region predicted by AlphaFold2. (**B**) Western blotting shows
1128 that anti-Daed monoclonal antibodies produced in this study are specific to Daed. Daed
1129 KD: Daed knockdown by RNAi. control: EGFP KD. β-Tub: loading control.

1130

1131 **Figure S2. Functions and behaviors of Daed and Gasz in OSCs**

1132 (**A**) Northern blotting using probes that detect *idefix* piRNA and *tj* piRNA. miR-310:
1133 loading control. KD: knockdown by RNAi. control: EGFP KD. pre-piRNA: piRNA
1134 precursors. (**B**) Western blotting shows the levels of Flag-Gasz WT and Flag-Gasz Δα-
1135 H2 where the same amounts of plasmids were used for transfection. β-Tub: loading
1136 control. The statistics of western blotting signals (n=3; left) and the mRNA expression
1137 levels (right). Signal intensities (left) or values (right) relative to F-Gasz WT were
1138 normalized with those of β-Tub or *rp49*, respectively, and presented as mean values ± SE.
1139 ***: p <0.005; n.s.: p >0.05 [*t*-test (unpaired, two-sided)]. (**C**) Western blotting shows
1140 HSP60 (a mitochondrial fraction marker) and β-Tub (a cytoplasmic fraction marker) in
1141 total lysates, and mitochondrial and cytoplasmic fractions in Figure 2G. (**D**) Summary of
1142 Armi subcellular localization in OSCs under each condition.

1143

1144 **Figure S3. Effects of Armi mutants on piRNA biogenesis and Piwi-piRISC function**

1145 (**A**) Peptide sequence and domain structure of Armi. The ATP binding residues and
1146 nucleotide binding residues are indicated in red and white, respectively. Asp1015,
1147 Arg1026, and Arg1037 are highlighted in blue. (**B**) Quantification of piRNA levels (n=3)
1148 (Figure 3H). Values relative to the control (EGFP KD) were normalized to Piwi level and
1149 presented as mean values ± SE. ***: $p < 0.005$; n.s.: $p > 0.05$ [*t*-test (unpaired, two-sided)].
1150 (**C**) This model summarizes the deleterious effects of Armi ΔN34 and KEE mutants on
1151 Armi–AmTEC interaction, piRNA biogenesis, and Piwi-piRISC function in OSCs. Blue
1152 arrowhead (WT): Zuc cleavage. Red arrowhead (KEE): obscured Zuc cleavage. White
1153 arrowhead (KEE): Zuc cleavage corresponding to WT.
1154
1155 **Figure S4. Effects of Daed and Armi mutants on piRNA biogenesis and Piwi-piRISC**
1156 **function**
1157 (**A**) Quantification of piRNA levels (n=3) (Figure 4A). Values relative to the control (EGFP
1158 KD) were normalized to Piwi level and presented as mean values ± SE. ***: $p < 0.005$; *:
1159 $p < 0.05$; [*t*-test (unpaired, two-sided)]. (**B**, **C**) Scatter plots showing the length distribution
1160 of piRNAs upon subdivision by target transposons (**B**) and the abundance of reads
1161 mapped antisense to transposons (**C**; Spearman's rho=0.98) in Daed WT and ΔSAM
1162 libraries. (**D**) Left: Piwi-bound piRNAs obtained from cytoplasmic fraction (Cyto) and
1163 nuclear extract fraction (Nuc). Immunoprecipitated Piwi was detected by western blotting.
1164 Right: Western blotting showing β-Tub (a cytoplasmic marker) and Histon H3 (a nucleus
1165 marker) in each fraction. (**E**) The expression levels of transposons (*gypsy*, *blood*, *gypsy5*,
1166 *quasimodo*, *17.6*, and *mdg3*) in control OSCs (dark gray), Daed-lacking OSCs (Daed
1167 KD; light gray), Flag-Daed WT rescued (WT; green) or Flag-Daed ΔSAM rescued cells
1168 (ΔSAM; red) (n=5). Values relative to the control (EGFP KD) were normalized to *rp49*

1169 and presented as mean values ± SE **: $p < 0.01$; n.s.: $p > 0.05$ [Wilcoxon rank sum exact
1170 test (two-sided)]. (**F**) Venn diagram showing the variety of positions of piRNA 5′ ends in
1171 the WT and ΔSAM libraries. (**G**) Heatmaps showing 5′ end counts of piRNAs mapped
1172 around the 10,000 most abundant piRNA 3′ ends (middle) and its binary histogram (top).
1173 In sequence logos (bottom), piRNAs were aligned according to the 3′ end of the piRNAs
1174 (black arrowhead) and its immediately downstream nucleotide is highlighted in green.
1175 Left: Daed ΔSAM Unchanged. Right: Daed ΔSAM Elongated. (**H**) piRNA production
1176 simulation. The U depletion in 29–34-nt piRNAs in WT and equivalent regions in ΔSAM
1177 are highlighted in yellow. (**I**) Length distribution of piRNAs (18–40 nt) in Armi WT (green)
1178 and KEE (red) libraries (n=3), presented as mean values ± SE. (**J**) Sequence logos
1179 representing 11 nt from the 5′ end of piRNAs in the Armi WT and KEE libraries. (**K**)
1180 Heatmaps showing the frequency of the 3′ end positions (red) corresponding to each 5′
1181 end of piRNAs in Armi WT (upper) and KEE (lower) libraries. The 50,000 piRNA 5′ end
1182 positions common to both libraries and most abundant in the WT library were used for
1183 analysis.
1184

1185 **Figure S5. Sequence alignment of Daed and Armi UPF1-like domain in species**

1186 (**A**, **B**) Phyrogenic tree (A) and multiple sequence alignment (B) of Daed orthologs
1187 constructed using Clustal Omega and MEGA 11. (**C**) Multiple sequence alignment of *D.*
1188 *melanogaster* Armi and its orthologs. Red arrowhead: Asp1015, Arg1026, and Arg1037
1189 (D-R-R) of *D. melanogaster* Armi.
1190

1191 **Figure S6. Reproducibility of piRNA-seq**

1192 (**A,B**) Scatter plots showing reproducibility of piRNA-seq of Daed WT, ΔSAM mutant (**A**),

1193 Armi WT and KEE mutant libraries (**B**). Gray dots indicate the number of normalized

1194 piRNA reads mapped to coding genes.

Figure 1

Koga et al.

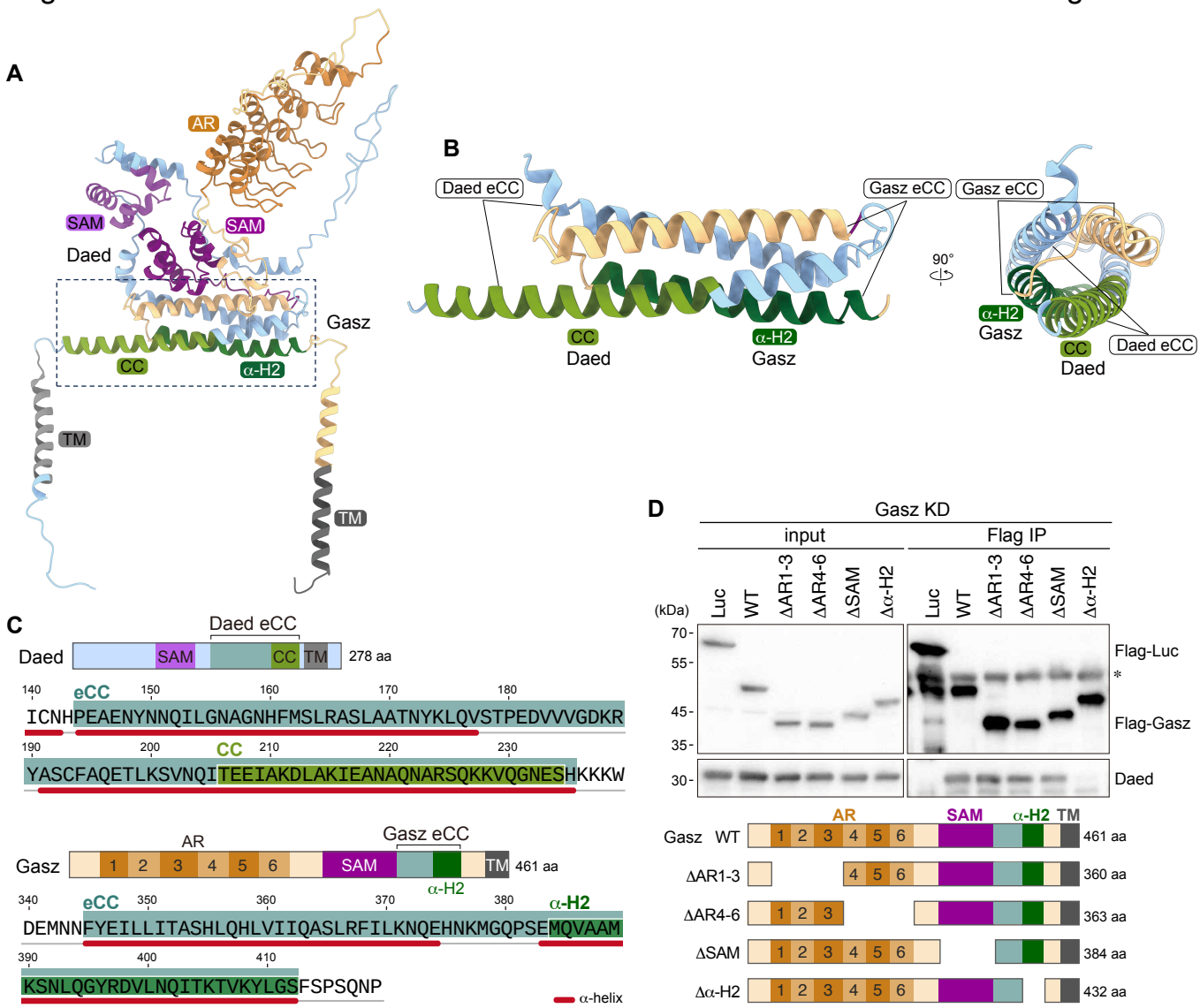

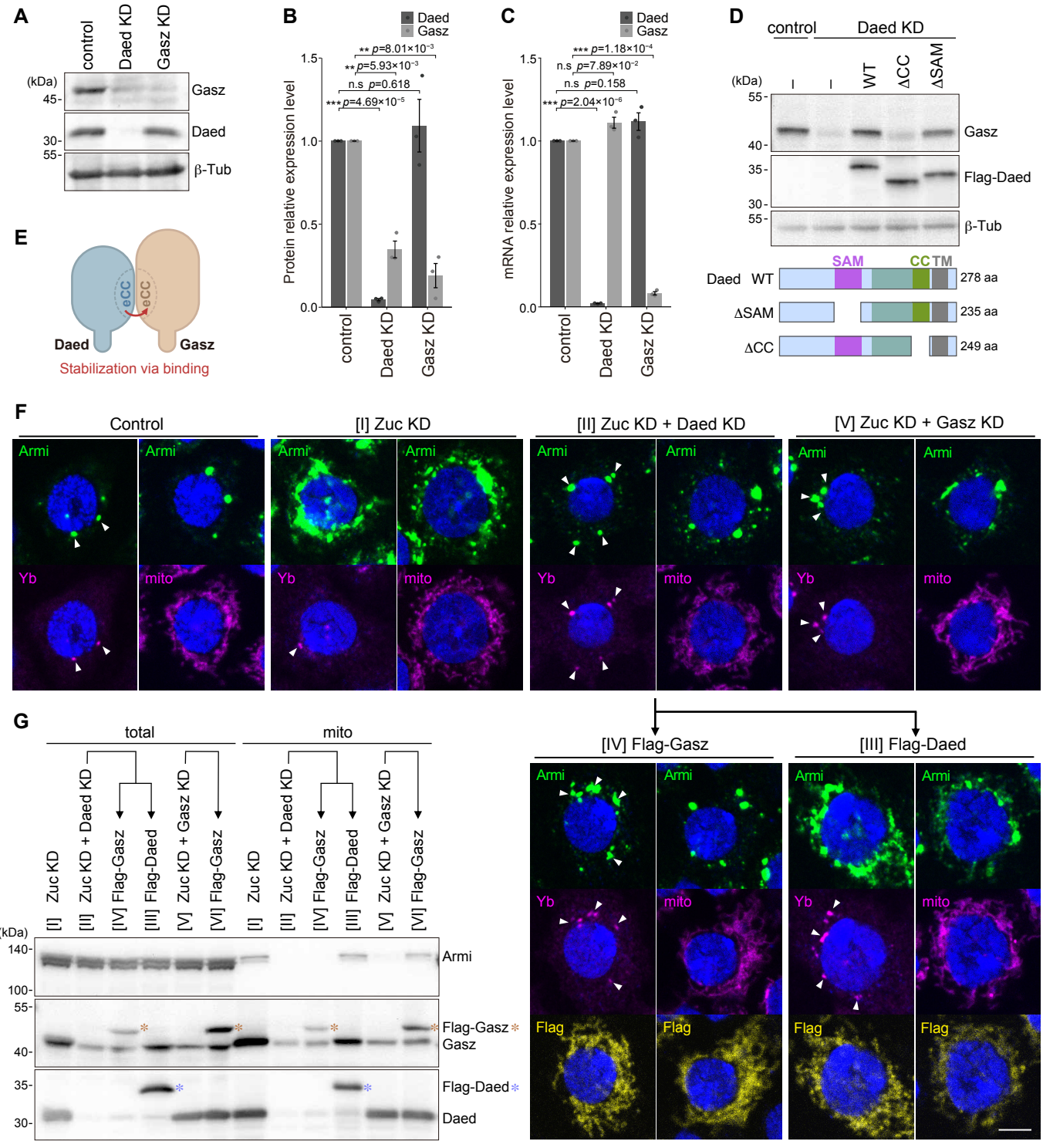
A
control
Daed KD
Gasz KD
(kDa)
45-
30-
55-
Gasz
Daed
β-Tub
B
Daed
Gasz
Protein relative expression level
** p=8.01×10⁻³
** p=5.93×10⁻³
n.s p=0.618
*** p=4.69×10⁻⁵
control
Daed KD
Gasz KD
C
mRNA relative expression level
*** p=1.18×10⁻⁴
n.s p=7.89×10⁻²
n.s p=0.158
*** p=2.04×10⁻⁶
D
control
Daed KD
WT
ΔCC
ΔSAM
Flag-Daed
β-Tub
SAM
CC
TM
Daed WT
278 aa
ΔSAM
235 aa
ΔCC
249 aa
E
eCC
Daed
Gasz
Stabilization via binding
F
Control
[I] Zuc KD
[II] Zuc KD + Daed KD
[V] Zuc KD + Gasz KD
Armi
Yb
mito
G
total
mito
[I] Zuc KD
[II] Zuc KD + Daed KD
[IV] Flag-Gasz
[III] Flag-Daed
[V] Zuc KD + Gasz KD
[VI] Flag-Gasz
Armi
Flag-Gasz
Gasz
Flag-Daed
Daed
[IV] Flag-Gasz
[III] Flag-Daed
Flag

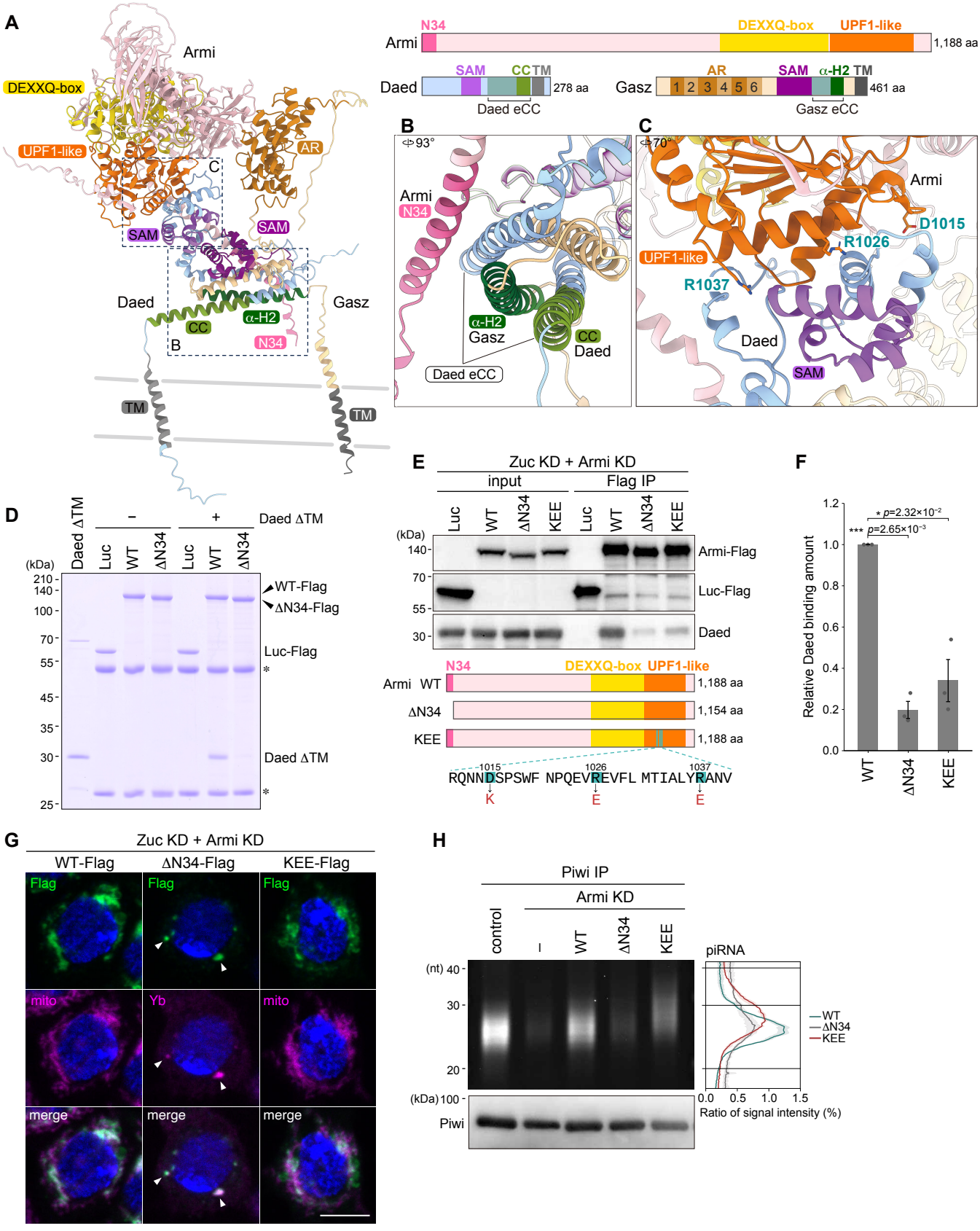
A
Armi
DEXXQ-box
UPF1-like
AR
C
SAM
SAM
Daed
Gasz
α-H2
CC
N34
B
TM
TM
N34
DEXXQ-box
UPF1-like
Armi
1,188 aa
Daed
SAM
CC TM
278 aa
Daed eCC
Gasz
AR
SAM
α-H2 TM
1 2 3 4 5 6
461 aa
Gasz eCC
B
93°
Armi
N34
α-H2
Gasz
CC
Daed
Daed eCC
C
70°
Armi
D1015
R1026
UPF1-like
R1037
Daed
SAM
D
Daed ΔTM
−
+
Daed ΔTM
Luc
WT
ΔN34
Luc
WT
ΔN34
(kDa)
210
140
100
70
55
45
35
30
25
WT-Flag
ΔN34-Flag
Luc-Flag
*
Daed ΔTM
*
E
Zuc KD + Armi KD
input
Flag IP
Luc
WT
ΔN34
KEE
Luc
WT
ΔN34
KEE
(kDa)
140
70
55
30
Armi-Flag
Luc-Flag
Daed
N34
DEXXQ-box
UPF1-like
Armi WT
1,188 aa
ΔN34
1,154 aa
KEE
1,188 aa
1015
1026
1037
RQNNDSPSWF NPQEVREVFL MTIALYRANV
K
E
E
F
Relative Daed binding amount
1.2
1.0
0.8
0.6
0.4
0.2
0.0
* p=2.32×10⁻²
*** p=2.65×10⁻³
WT
ΔN34
KEE
G
Zuc KD + Armi KD
WT-Flag
ΔN34-Flag
KEE-Flag
Flag
Flag
Flag
mito
Yb
mito
merge
merge
merge
H
Piwi IP
Armi KD
control
−
WT
ΔN34
KEE
(nt) 40
30
20
(kDa) 100
Piwi
piRNA
WT
ΔN34
KEE
0.0
0.5
1.0
1.5
Ratio of signal intensity (%)

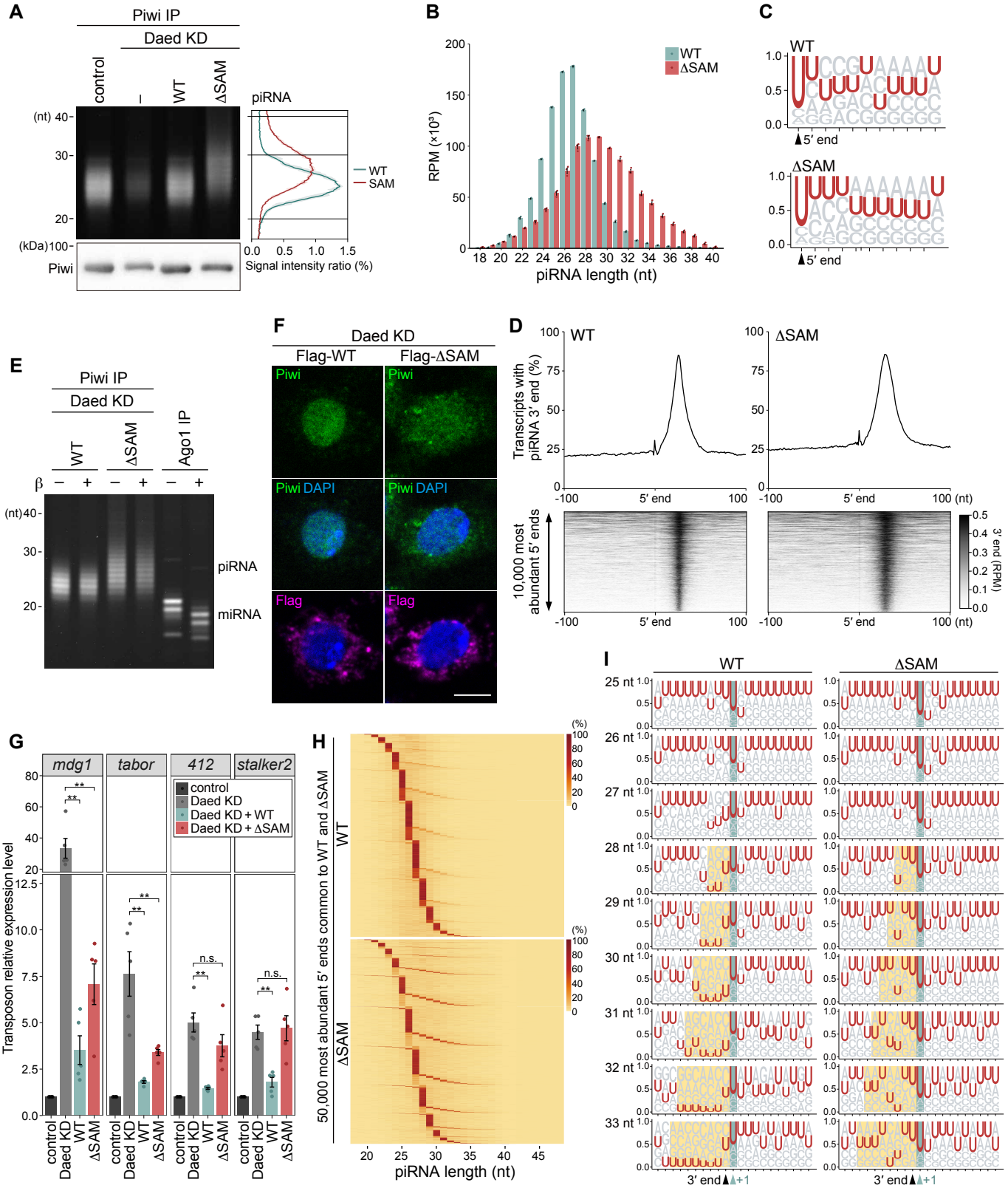
A
Piwi IP
Daed KD
control
I
WT
ΔSAM
(nt) 40
30
20
(kDa) 100
Piwi
piRNA
WT
SAM
0.0 0.5 1.0 1.5
Signal intensity ratio (%)
B
WT
ΔSAM
RPM (×10³)
piRNA length (nt)
C
WT
ΔSAM
5′ end
D
WT
ΔSAM
Transcripts with piRNA 3′ end (%)
10,000 most abundant 5′ ends
5′ end
3′ end (RPM)
E
Piwi IP
Daed KD
WT
ΔSAM
Ago1 IP
β
(nt) 40
30
20
piRNA
miRNA
F
Daed KD
Flag-WT
Flag-ΔSAM
Piwi
Piwi DAPI
Flag
G
mdg1
tabor
412
stalker2
control
Daed KD
Daed KD + WT
Daed KD + ΔSAM
Transposon relative expression level
n.s.
H
50,000 most abundant 5′ ends common to WT and ΔSAM
WT
ΔSAM
(%)
piRNA length (nt)
I
WT
ΔSAM
25 nt
26 nt
27 nt
28 nt
29 nt
30 nt
31 nt
32 nt
33 nt
3′ end
+1

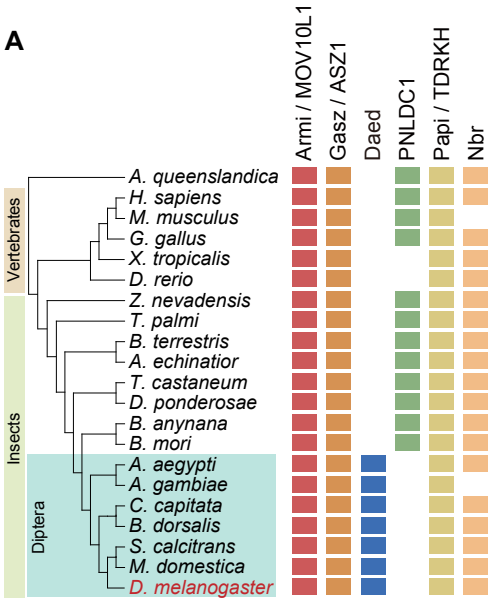
A
Armi / MOV10L1
Gasz / ASZ1
Daed
PNLDC1
Papi / TDRKH
Nbr
Vertebrates
Insects
Diptera
A. queenslandica
H. sapiens
M. musculus
G. gallus
X. tropicalis
D. rerio
Z. nevadensis
T. palmi
B. terrestris
A. echinatior
T. castaneum
D. ponderosae
B. anynana
B. mori
A. aegypti
A. gambiae
C. capitata
B. dorsalis
S. calcitrans
M. domestica
D. melanogaster

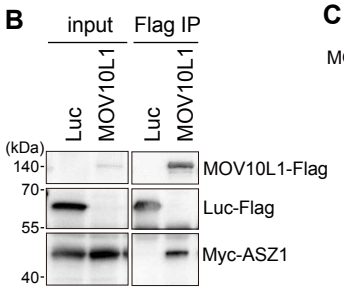
B
input
Flag IP
Luc
MOV10L1
Luc
MOV10L1
(kDa)
140-
70-
55-
40-
MOV10L1-Flag
Luc-Flag
Myc-ASZ1

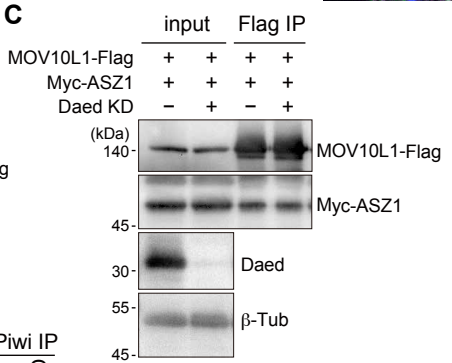
C
input
Flag IP
MOV10L1-Flag + + + +
Myc-ASZ1 + + + +
Daed KD − + − +
(kDa)
140-
45-
30-
55-
45-
MOV10L1-Flag
Myc-ASZ1
Daed
β-Tub

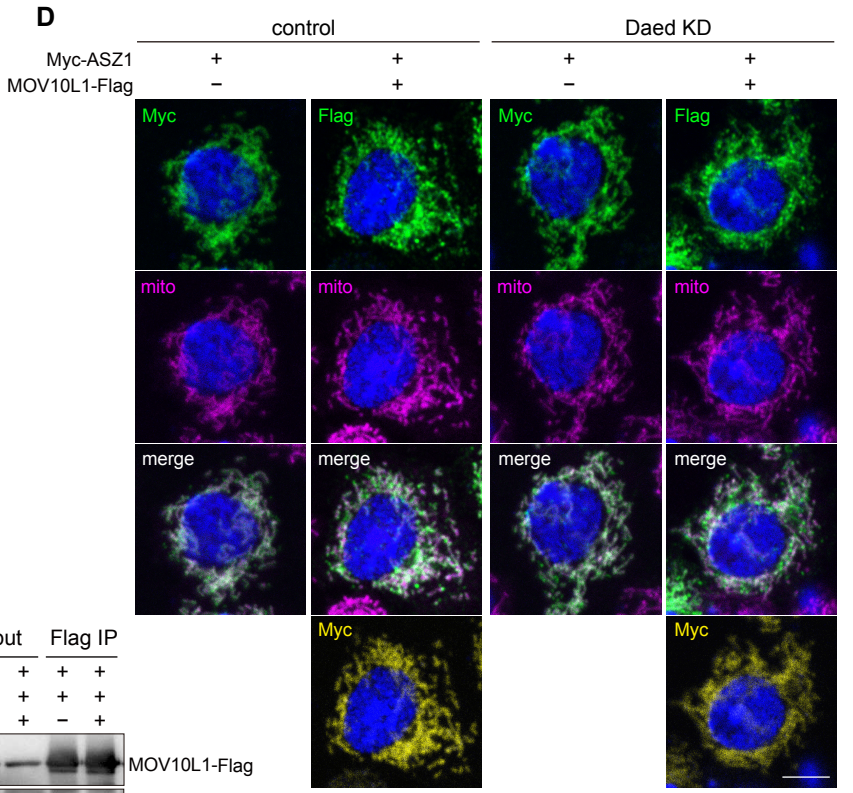
D
control
Daed KD
Myc-ASZ1 + + + +
MOV10L1-Flag − + − +
Myc
Flag
mito
merge

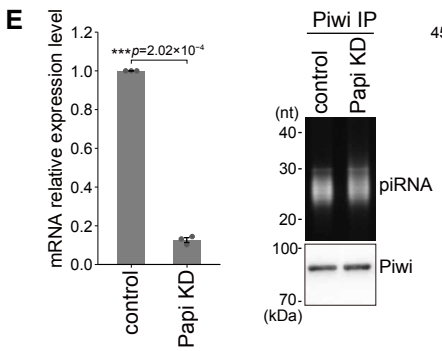
E
mRNA relative expression level
***p=2.02×10⁻⁴
1.2
1.0
0.8
0.6
0.4
0.2
0.0
control
Papi KD
Piwi IP
control
Papi KD
(nt)
40-
30-
20-
piRNA
100-
70-
(kDa)
Piwi

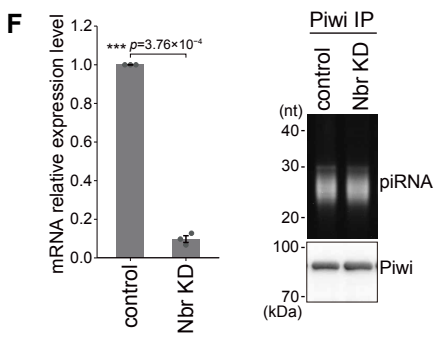
F
mRNA relative expression level
*** p=3.76×10⁻⁴
1.2
1.0
0.8
0.6
0.4
0.2
0.0
control
Nbr KD
Piwi IP
control
Nbr KD
(nt)
40-
30-
20-
piRNA
100-
70-
(kDa)
Piwi

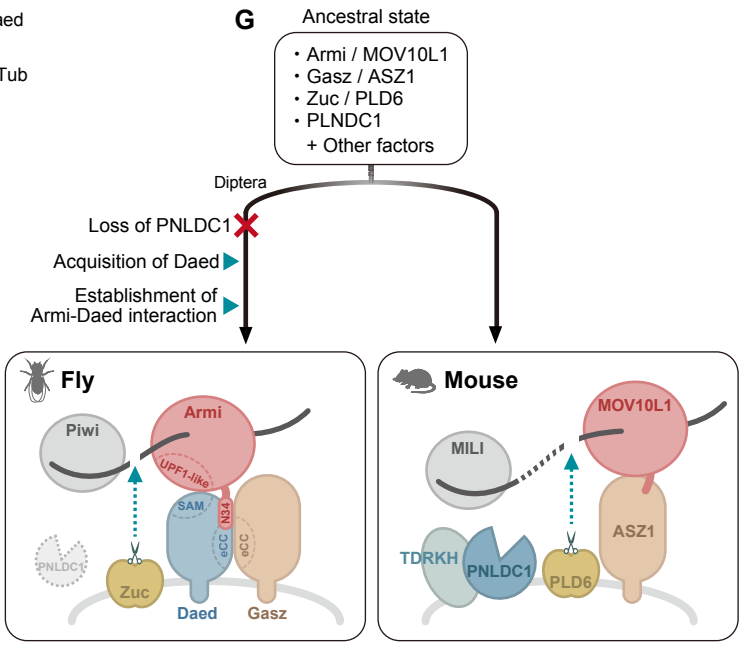
G
Ancestral state
• Armi / MOV10L1
• Gasz / ASZ1
• Zuc / PLD6
• PLNDC1
+ Other factors
Diptera
Loss of PNLDC1
Acquisition of Daed
Establishment of
Armi-Daed interaction
Fly
Piwi
Armi
UPF1-like
SAM
N34
eCC
eCC
PNLDC1
Zuc
Daed
Gasz
Mouse
MILI
MOV10L1
ASZ1
TDRKH
PNLDC1
PLD6

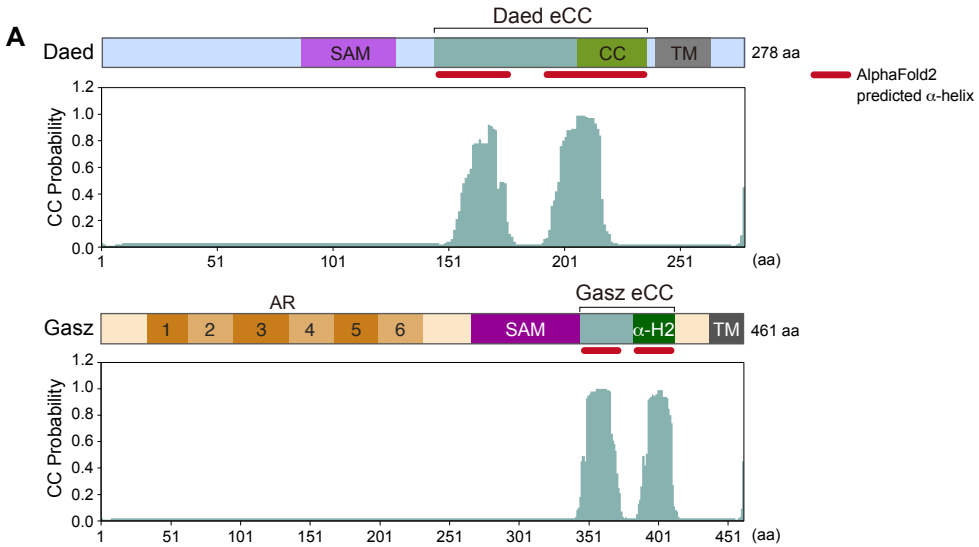
A
Daed eCC
Daed
SAM
CC
TM
278 aa
AlphaFold2 predicted α-helix
CC Probability
1.2
1.0
0.8
0.6
0.4
0.2
0.0
1
51
101
151
201
251
(aa)
AR
Gasz eCC
Gasz
1
2
3
4
5
6
SAM
α-H2
TM
461 aa
CC Probability
1
51
101
151
201
251
301
351
401
451
(aa)

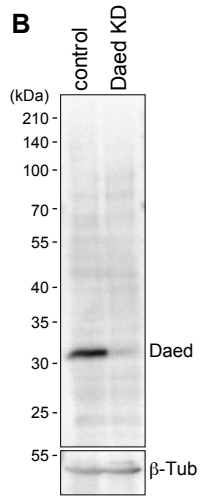
B
control
Daed KD
(kDa)
210
140
100
70
55
40
35
30
25
55
Daed
β-Tub

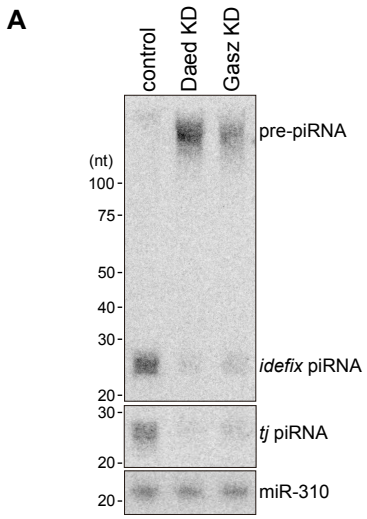

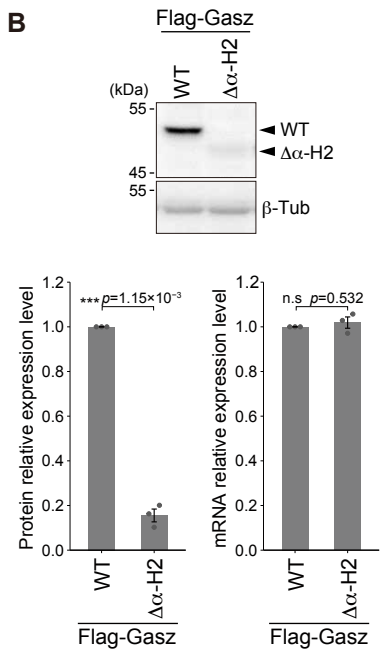

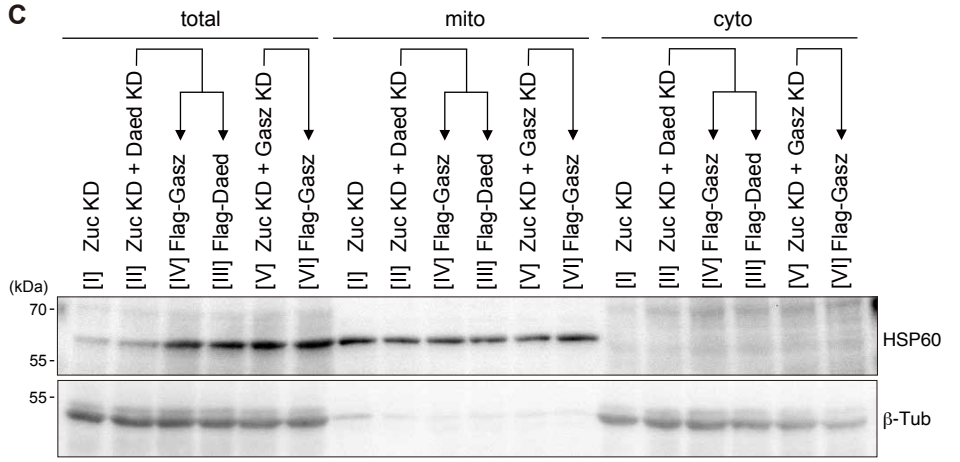

D

	Armi	Daed	Gasz
Control	Yb body	+	+
[I] Zuc KD	mitochondria	+	+
[II] ZucKD + Daed KD	Yb body	–	–
[III] ZucKD + Daed KD, Flag-Daed	mitochondria	+	+
[IV] ZucKD + Daed KD, Flag-Gasz	Yb body	–	+
[V] ZucKD + Gasz KD	Yb body	+	–
[VI] ZucKD + Gasz KD, Flag-Gasz	mitochondria	+	+

A

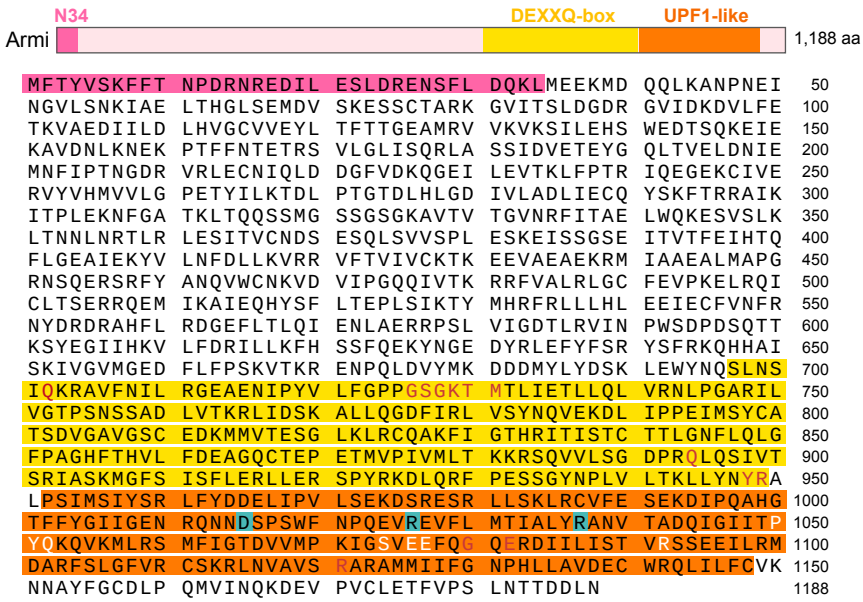
N34
DEXXQ-box
UPF1-like
Armi
1,188 aa
MFTYVSKFFT NPDRNREDIL ESLDRENSFL DQKLMEEKMD QQLKANPNEI 50
NGVLSNKIAE LTHGLSEMDV SKESSCTARK GVITSLDGDR GVIDKDVLFE 100
TKVAEDIILD LHVGCVVEYL TFTTGEAMRV VKVKSILEHS WEDTSQKEIE 150
KAVDNLKNEK PTFFNTETRS VLGLISQRLA SSIDVETEYG QLTVELDNIE 200
MNFIPTNGDR VRLECNIQLD DGFVDKQGEI LEVTKLFPTR IQEGEKCIVE 250
RVYVHMVVLG PETYILKTDL PTGTDLHLGD IVLADLIECQ YSKFTRRAIK 300
ITPLEKNFGA TKLTQQSSMG SSGSGKAVTV TGVNRFITAE LWQKESVSLK 350
LTNNLNRTLR LESITVCNDS ESQLSVVSPL ESKEISSGSE ITVTFEIHTQ 400
FLGEAIEKYV LNFDLLKVRR VFTVIVCKTK EEVAEAEKRM IAAEALMAPG 450
RNSQERSRFY ANQVWCNKVD VIPGQQIVTK RRFVALRLGC FEVPKELRQI 500
CLTSERRQEM IKAIEQHYSF LTEPLSIKTY MHRFRLLLHL EEIECFVNFR 550
NYDRDRAHFL RDGEFLTLQI ENLAERRPSL VIGDTLRVIN PWSDPDSQTT 600
KSYEGIIHKV LFDRILLKFH SSFQEKYNGE DYRLEFYFSR YSFRKQHHAI 650
SKIVGVMGED FLFPSKVTKR ENPQLDVYMK DDDMYLYDSK LEWYNQSLNS 700
IQKRAVFNIL RGEAENIPYV LFGPPGSGKT MTLIETLLQL VRNLPGARIL 750
VGTPSNSSAD LVTKRLIDSK ALLQGDFIRL VSYNQVEKDL IPPEIMSYCA 800
TSDVGAVGSC EDKMMVTESG LKLRCQAKFI GTHRITISTC TTLGNFLQLG 850
FPAGHFTHVL FDEAGQCTEP ETMVPIVMLT KKRSQVVLSG DPRQLQSIVT 900
SRIASKMGFS ISFLERLLER SPYRKDLQRF PESSGYNPLV LTKLLYNYRA 950
LPSIMSIYSR LFYDDELIPV LSEKDSRESR LLSKLRCVFE SEKDIPQAHG 1000
TFFYGIIGEN RQNNDSPSWF NPQEVREVFL MTIALYRANV TADQIGIITP 1050
YQKQVKMLRS MFIGTDVVMP KIGSVEEFQG QERDIILIST VRSSEEILRM 1100
DARFSLGFVR CSKRLNVAVS RARAMMIIFG NPHLLAVDEC WRQLILFCVK 1150
NNAYFGCDLP QMVINQKDEV PVCLETFVPS LNTTDDLN 1188

B

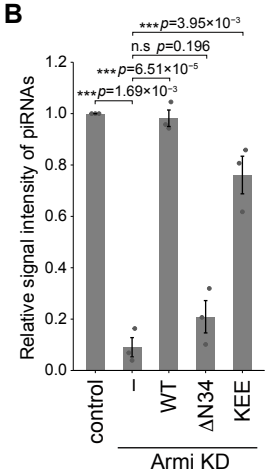
***p=3.95×10⁻³
n.s p=0.196
***p=6.51×10⁻⁵
***p=1.69×10⁻³
Relative signal intensity of piRNAs
1.2
1.0
0.8
0.6
0.4
0.2
0.0
control
–
WT
ΔN34
KEE
Armi KD

C

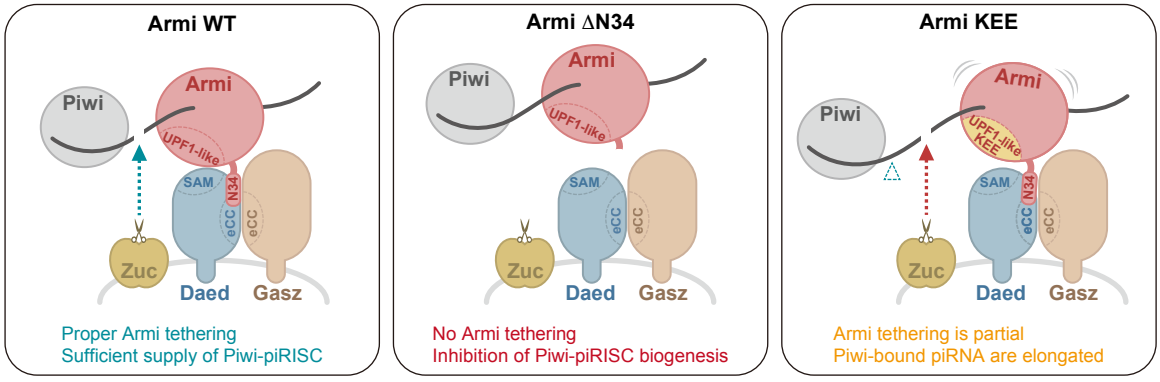
Armi WT
Piwi
Armi
UPF1-like
SAM
N34
eCC
eCC
Zuc
Daed
Gasz
Proper Armi tethering
Sufficient supply of Piwi-piRISC
Armi ΔN34
Piwi
Armi
UPF1-like
SAM
eCC
eCC
Zuc
Daed
Gasz
No Armi tethering
Inhibition of Piwi-piRISC biogenesis
Armi KEE
Piwi
Armi
UPF1-like
KEE
SAM
N34
eCC
eCC
Zuc
Daed
Gasz
Armi tethering is partial
Piwi-bound piRNA are elongated

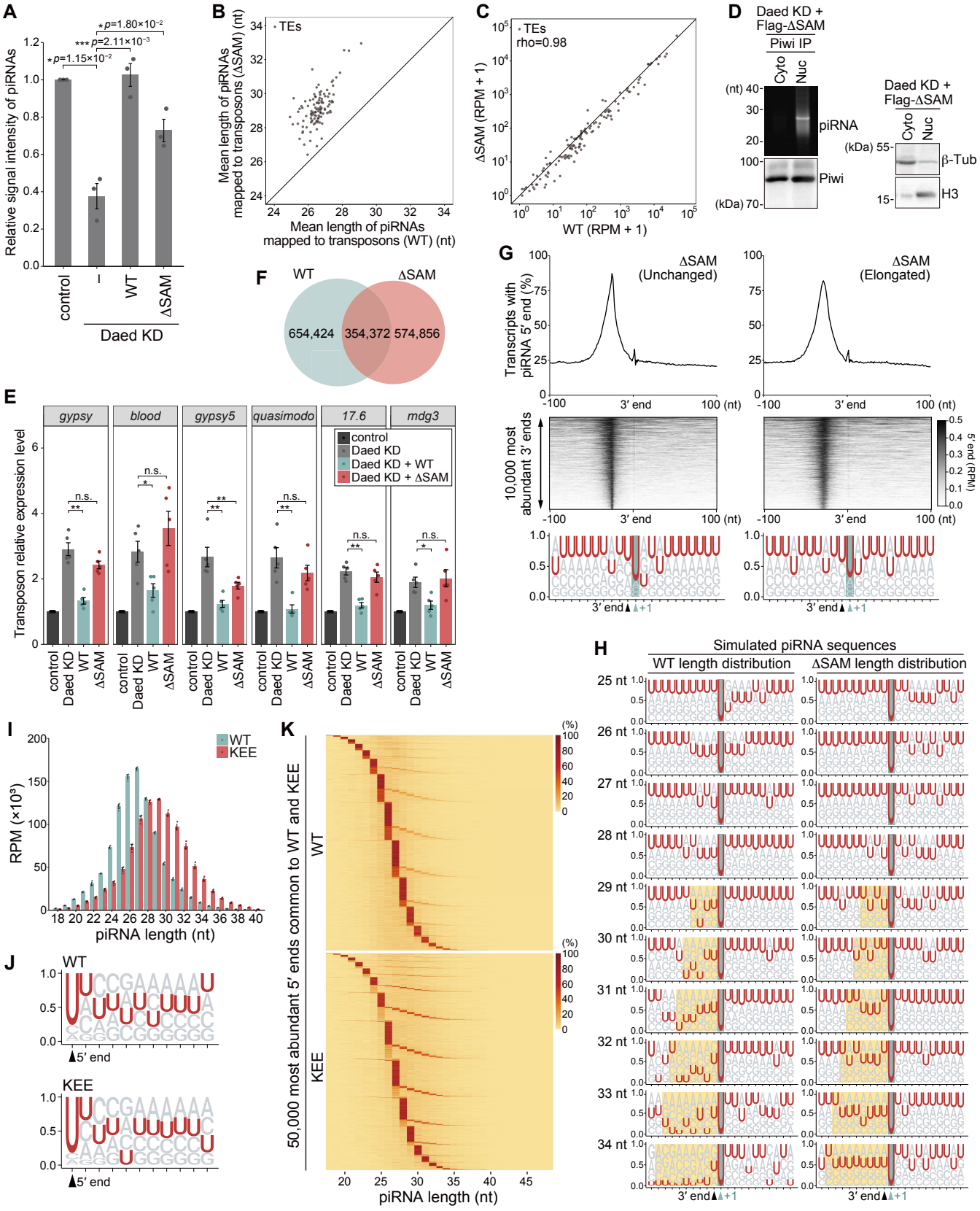
A
Relative signal intensity of piRNAs
*p=1.15×10⁻²
***p=2.11×10⁻³
*p=1.80×10⁻²
control
I
WT
ΔSAM
Daed KD
B
TEs
Mean length of piRNAs mapped to transposons (ΔSAM) (nt)
Mean length of piRNAs mapped to transposons (WT) (nt)
C
TEs
rho=0.98
ΔSAM (RPM + 1)
WT (RPM + 1)
D
Daed KD + Flag-ΔSAM
Piwi IP
Cyto
Nuc
(nt)
piRNA
Piwi
(kDa)
Daed KD + Flag-ΔSAM
β-Tub
H3
F
WT
ΔSAM
654,424
354,372
574,856
G
ΔSAM (Unchanged)
ΔSAM (Elongated)
Transcripts with piRNA 5′ end (%)
3′ end
10,000 most abundant 3′ ends
5′ end (RPM)
E
gypsy
blood
gypsy5
quasimodo
17.6
mdg3
Transposon relative expression level
control
Daed KD
Daed KD + WT
Daed KD + ΔSAM
n.s.
H
Simulated piRNA sequences
WT length distribution
ΔSAM length distribution
25 nt
26 nt
27 nt
28 nt
29 nt
30 nt
31 nt
32 nt
33 nt
34 nt
3′ end
I
WT
KEE
RPM (×10³)
piRNA length (nt)
J
WT
KEE
5′ end
K
50,000 most abundant 5′ ends common to WT and KEE
WT
KEE
(%)
piRNA length (nt)

A

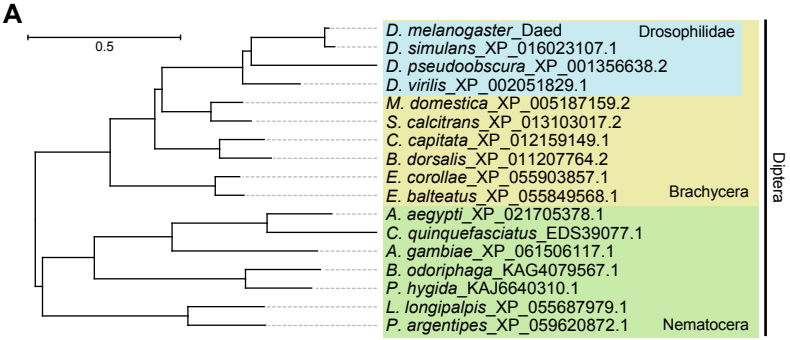
0.5
D. melanogaster_Daed
D. simulans_XP_016023107.1
D. pseudoobscura_XP_001356638.2
D. virilis_XP_002051829.1
M. domestica_XP_005187159.2
S. calcitrans_XP_013103017.2
C. capitata_XP_012159149.1
B. dorsalis_XP_011207764.2
E. corollae_XP_055903857.1
E. balteatus_XP_055849568.1
A. aegypti_XP_021705378.1
C. quinquefasciatus_EDS39077.1
A. gambiae_XP_061506117.1
B. odoriphaga_KAG4079567.1
P. hygida_KAJ6640310.1
L. longipalpis_XP_055687979.1
P. argentipes_XP_059620872.1
Drosophilidae
Brachycera
Nematocera
Diptera

B

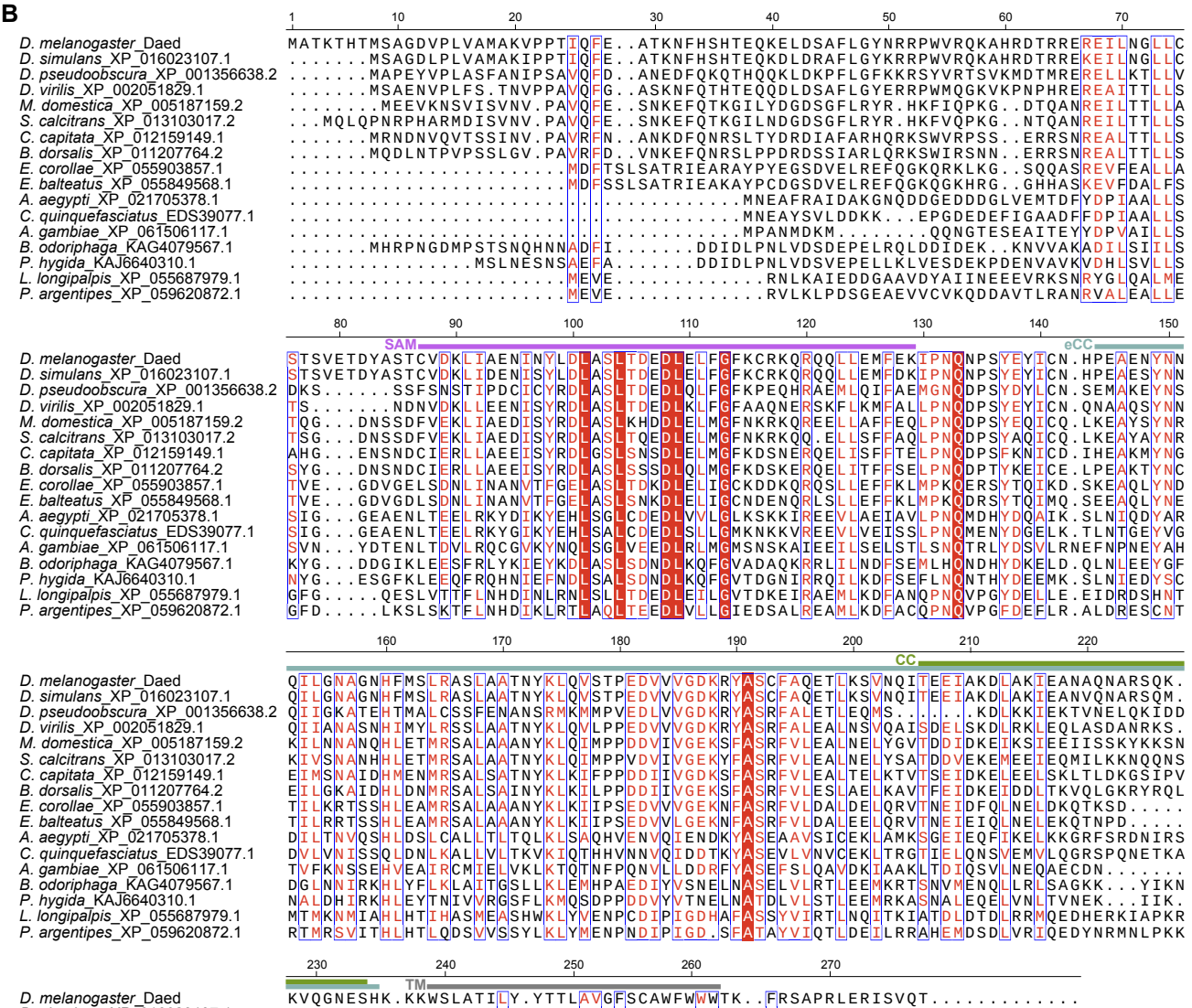
SAM
eCC
CC
TM

c

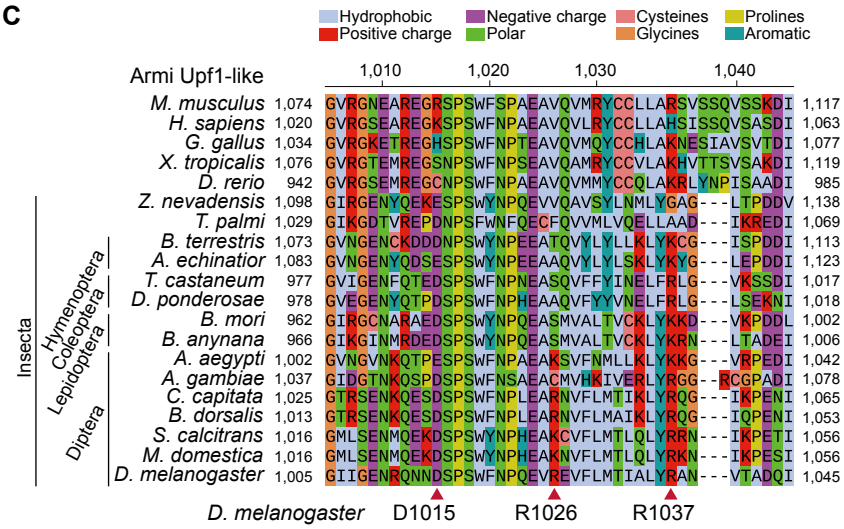
Hydrophobic
Positive charge
Negative charge
Polar
Cysteines
Glycines
Prolines
Aromatic
Armi Upf1-like
1,010
1,020
1,030
1,040
M. musculus 1,074 GVRGNEAREGRSPSWFSPAEAVQVMRYCCLLARSVSSQVSSKDI 1,117
H. sapiens 1,020 GVRGSEAREGKSPSWFNPAEAVQVLRYCCLLAHSISSQVSASDI 1,063
G. gallus 1,034 GVRGKETREGHSPSWFNPTEAVQVMQYCCHLAKNESIAVSVTDI 1,077
X. tropicalis 1,076 GVRGTEMREGSNPSWFNPSEAVQAMRYCCVLAKHVTTSVSAKDI 1,119
D. rerio 942 GVRGSEMREGCNPSWFNPAEAVQVMMYCCQLAKRLYNPISAADI 985
Z. nevadensis 1,098 GIRGENYQEKESPSWYNPQEVVQAVSYLNMLYGAG---LTPDDV 1,138
T. palmi 1,029 GIKGDTVREPDNPSFWNFQECFQVVMLVQELLAAD---IKREDI 1,069
B. terrestris 1,073 GVNGENCKDDDNPSWYNPEEATQVYLYLLKLYKCG---ISPDDI 1,113
A. echinatior 1,083 GVNGENYQDSESPSWYNPEEAAQVYLYLSKLYKYG---LEPDDI 1,123
T. castaneum 977 GVIGENFQTEDSPSWFNPNEASQVFFYINELFRLG---VKSSDI 1,017
D. ponderosae 978 GVEGENYQTPDSPSWFNPHEAAQVFYYVNELFRLG---LSEKNI 1,018
B. mori 962 GIRGCNARAEDSPSWYNPQEASMVALTVCKLYKKD---VKPDDL 1,002
B. anynana 966 GIKGINMRDEDSPSWYNPQEASMVALTVCKLYKRN---LTADEI 1,006
A. aegypti 1,002 GVNGVNKQTPESPSWFNPAEAKSVFNMLLKLYKKG---VRPEDI 1,042
A. gambiae 1,037 GIDGTNKQSPDSPSWFNSAEACMVHKIVERLYRGG--RCGPADI 1,078
C. capitata 1,025 GTRSENKQESDSPSWFNPLEARNVFLMTIKLYRQG---IKPENI 1,065
B. dorsalis 1,013 GTRSENKQESDSPSWFNPLEARNVFLMAIKLYRQG---IQPENI 1,053
S. calcitrans 1,016 GMLSENMQEKDSPSWYNPHEAKCVFLMTLQLYRRN---IKPETI 1,056
M. domestica 1,016 GMLSENMQEKDSPSWYNPHEAKNVFLMTLQLYRKN---IKPESI 1,056
D. melanogaster 1,005 GIIGENRQNNDSPSWFNPQEVREVFLMTIALYRAN---VTADQI 1,045
Insecta
Hymenoptera
Coleoptera
Lepidoptera
Diptera
D. melanogaster D1015 R1026 R1037

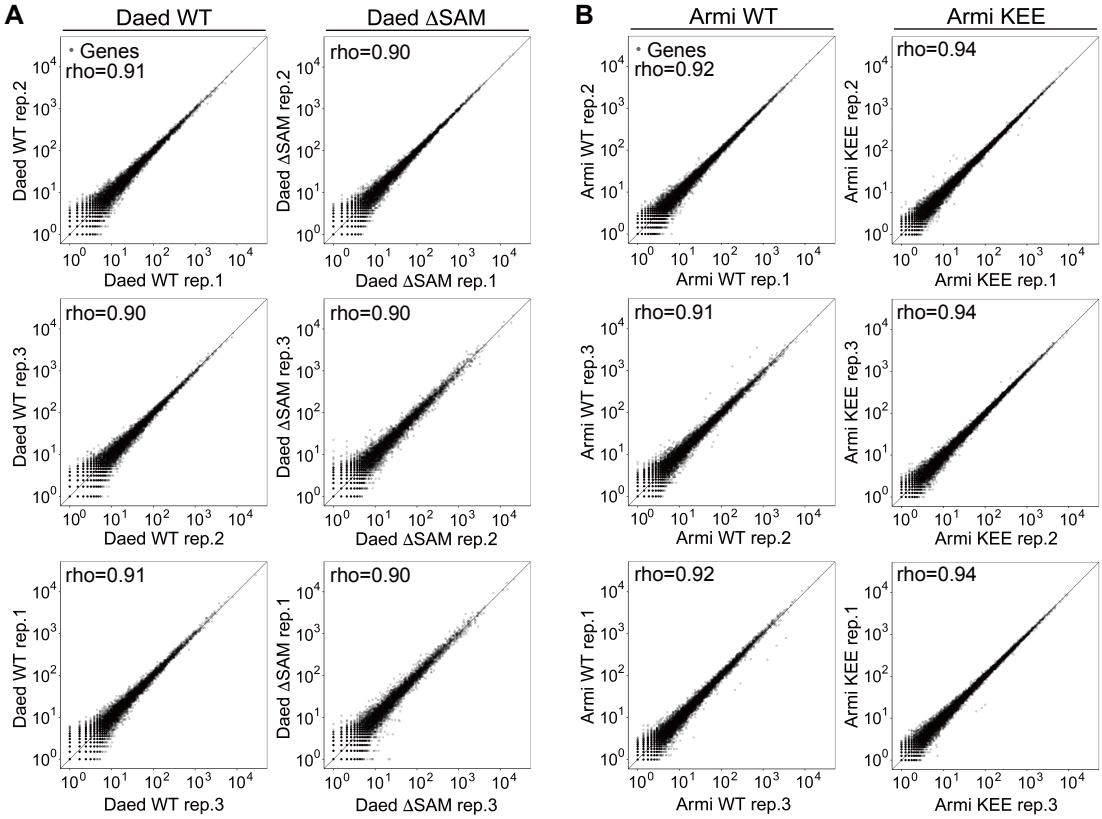
A
Daed WT
Daed ΔSAM
Genes
rho=0.91
rho=0.90
rho=0.90
rho=0.90
rho=0.91
rho=0.90
Daed WT rep.1
Daed WT rep.2
Daed WT rep.3
Daed ΔSAM rep.1
Daed ΔSAM rep.2
Daed ΔSAM rep.3
B
Armi WT
Armi KEE
Genes
rho=0.92
rho=0.94
rho=0.91
rho=0.94
rho=0.92
rho=0.94
Armi WT rep.1
Armi WT rep.2
Armi WT rep.3
Armi KEE rep.1
Armi KEE rep.2
Armi KEE rep.3

Table S1. Primer sequences for plasmid construction

name	primer sequence	plasmid
Daed-clonig-insert_F	CTTGGTACCGAATTCATGGCAACGAAGACGCACAC	pAc-Flag-Daed
Daed-clonig-insert_R	GACTCGAGCGGCCGCTTAAGTCTGAACGGAGATCC	pAc-Flag-Daed
Daed-clonig-vector_F	TAAGCGGCCGCTCGAGTCTA	pAc-Flag-Daed
Daed-clonig-vector_R	CATGAATTCGGTACCAAGCT	pAc-Flag-Daed
Flag-Luc_insert_F	ATGGACTACAAAGACCATGACG	pAc-Flag-Luc
Flag-Luc_insert_R	CTTGTCATCGTCATCCTTGT	pAc-Flag-Luc
Flag-Luc_vector_F	GTCTTTGTAGTCCATGGTGGCTAGCCCGAT	pAc-Flag-Luc
Flag-Luc_vector_R	GGATGACGATGACAAGATGGAAGACGCCAAAAACATAAAGAAAG	pAc-Flag-Luc
Flag-Daed (RNAi resistant)_F	GATAAGCTCATTGCCGAGAACATT	pAc-Flag-Daed (RNAi resistant)
Flag-Daed (RNAi resistant)_R	AACGCATGTACTGGCGTAGTCC	pAc-Flag-Daed (RNAi resistant)
Flag-Daed ΔSAM_F	ATTCCCAACCAGAATCCCAGTTACG	pAc-Flag-Daed ΔSAM
Flag-Daed ΔSAM_R	TGTACTGGCGTAGTCCGTTTCCACG	pAc-Flag-Daed ΔSAM
Flag-Daed ΔCC_F	CACAAGAAGAAGAAGTGGAGCCTGG	pAc-Flag-Daed ΔCC
Flag-Daed ΔCC_R	GATCTGATTCACGCTTTTTAGAGTT	pAc-Flag-Daed ΔCC
GST-Daed_full_length_insert_F	GGGCCCCTGGGATCCATGGCAACGAAGACGCACAC	pGEX-GST-Daed
GST-Daed_full_length_insert_R	ACCCGGGAATTCCGGTTAAGTCTGAACGGAGATCC	pGEX-GST-Daed
GST-Daed_full_length_vector_F	CCGGAATTCCCGGGTCGACTCGAGC	pGEX-GST-Daed
GST-Daed_full_length_vector_R	GGATCCCAGGGGCCCCTGGAACAGA	pGEX-GST-Daed
GST-Daed ΔTM_F	TGGACCAAGTTCCGCAGCGCTCCCC	pGEX-GST-Daed ΔTM
GST-Daed ΔTM_R	CTTCTTCTTCTTGTGACTCTCGTTG	pGEX-GST-Daed ΔTM
GST-Daed ΔTM-His_F	CATCATCACTAACCGGAATTCCCGG	pGEX-GST-Daed ΔTM-His
GST-Daed ΔTM-His_R	ATGATGATGAGTCTGAACGGAGATC	pGEX-GST-Daed ΔTM-His
GST-Daed (N1-197)_insert_F	GGGCCCCTGGGATCCATGGCAACGAAGACGCA	pGEX-GST-Daed (N1-197)
GST-Daed (N1-197)_insert_R	ACCCGGGAATTCCGGTTATTCCTGGGCAAAGCAG	pGEX-GST-Daed (N1-197)
GST-Daed (N1-197)_vector_F	CCGGAATTCCCGGGT	pGEX-GST-Daed (N1-197)
GST-Daed (N1-197)_vector_R	GGATCCCAGGGGCC	pGEX-GST-Daed (N1-197)
Flag-Gasz ΔAR1-3_F	CACGGAGCCGTGATCAATGTTTCGG	pAc-Flag-Gasz ΔAR1-3
Flag-Gasz ΔAR1-3_R	CTTGGAGCGTTTCACCTCATCCGAG	pAc-Flag-Gasz ΔAR1-3
Flag-Gasz ΔAR4-6_F	CCAGCCTCCACTTACCTAGTGCCGA	pAc-Flag-Gasz ΔAR4-6
Flag-Gasz ΔAR4-6_R	CCGCAAGAGCAGGCCCACAATTCTC	pAc-Flag-Gasz ΔAR4-6
Flag-Gasz ΔSAM_F	TTCTATGAGATCCTACTGATCACCG	pAc-Flag-Gasz ΔSAM
Flag-Gasz ΔSAM_R	TTGAAAATATTCCGGGCAATCGCTC	pAc-Flag-Gasz ΔSAM
Flag-Gasz ΔCC_F	TTTAGCCCCTCTCAGAATCCCTTGT	pAc-Flag-Gasz ΔCC
Flag-Gasz ΔCC_R	CTCCGAAGGTTGCCCCATTTTATTG	pAc-Flag-Gasz ΔCC
Armi D1015K-Flag_F	ATAACAAATCaCCTTCCTGGTTCAA	pAc-Armi KEE-Flag
Armi D1015K-Flag_R	TTTGCCTGTTTTCGCCAATGATTCC	pAc-Armi KEE-Flag
Armi R1026E-Flag_F	AATCCCCAAGAGGTCGAGGAGGTGT	pAc-Armi KEE-Flag
Armi R1026E-Flag_R	GAACCAGGAAGGTGAATCGTTATTT	pAc-Armi KEE-Flag
Armi R1037E-Flag_F	ACGAGGCCAATGTGACTGCCGATCA	pAc-Armi KEE-Flag
Armi R1037E-Flag_R	ACAGGGCGATGGTCATTAGGAACAC	pAc-Armi KEE-Flag
MOV10L1-clonig-insert_F	ATCGGGCTAGCCACCATGCTGCGCCTTGCTGCCAA	pAc-MOV10L1-Flag
MOV10L1-clonig-insert_R	TTTGTAGTCCTCGAGCTTTTGGAGAGCCTGGAGTT	pAc-MOV10L1-Flag
MOV10L1-clonig-vector_F	CTCGAGGACTACAAAGACCATGACG	pAc-MOV10L1-Flag
MOV10L1-clonig-vector_R	CATGGTGGCTAGCCCGATCCGGGGT	pAc-MOV10L1-Flag
ASZ1-clonig-insert_F	GGTACCGAATTCATGGCAGCGGGCACACTGAGGGG	pAc-Myc-ASZ1
ASZ1-clonig-insert_R	TCGAGCGGCCGCTTATTTTCTCTGCAAAGTTAGCT	pAc-Myc-ASZ1
ASZ1-clonig-vector_F	TAAGCGGCCGCTCGAGTCTAGAGGG	pAc-Myc-ASZ1
ASZ1-clonig-vector_R	CATGAATTCGGTACCAAGCTTGTTC	pAc-Myc-ASZ1

Table S2. siRNA sequences

name	sense	antisense
siEGFP	*GGCAAGCUGACCCUGAAGU*TT	*ACUUCAGGGUCAGCUUGCC*TT
siDaed	*CCUGUGUGGACAAACUUAUUG*	*AUAAGUUUGUCCACACAGGUG*
siGasz	*CGCUCGAAACCAGCUCCUU*TT	*AAGGAGCUGGUUUCGAGCG*TT
siArmi	*CAGCUUAAGGCGAAUCCAA*TT	*UUGGAUUCGCCUUAAGCUG*TT
siZuc	*GCAUUGCCGUCAGCACUGU*TT	*ACAGUGCUGACGGCAAUGC*TT
siPapi	*GAUUACGAGACAAAGACAG*TT	*CUGUCUUUGUCUCGUAAUC*TT
siNbr	*CCTAATGAGCAACCTGAAG*TT	*CTTCAGGTTGCTCATTAGG*TT

*: RNA is shown in itallics

Table S3. Probe sequences for northern blotting

name	probe sequence
idefix-piRNA	AAACTACTGGCAATCGTTTGGGAA
tj-piRNA	GGTAATGGGAATGCACTTCTCTTGAA
miR-310	AAAGGCCGGGAAGTGTGCAATA

Table S4. Primer sequences for qPCR

name	forward primer (5′ > 3′)	reverse primer (5′ > 3′)
rp49	CCGCTTCAAGGGACAGTATCTG	ATCTCGCCGCAGTAAACGC
Daed	GCAACGAAGACGCACACAAT	TCGGTGTGCGAGTGAAAGTT
Gasz	ACTTCCTGGGCTACAACACG	GGCCTCCAGTATGCCGTTAA
Flag-Gasz	ATGGACTACAAAGACCATGACGGTG	GAGCAGGCCCACAATTCTCTCCGCC
Nbr	GCCTTGGCAAGAAACTGAAC	ACCCCGCCTGAGAAAGTTAT
mdg1	AACAGAAACGCCAGCAACAGC	CGTTCCCATGTCCGTTGTGAT
tabor	ACAACAGAAGCCGCAAACTG	CAGCTATTGTGAGTGGGCGT
412	ATGCCACTGGTCTAAGCACC	ATAGTGGTGCAAGTCCCTGC
stalker2	CACACAGAAGAACAAGCGGC	TTAACCGCAACGCTTCCTCT
gypsy	CCAGGTCGGGCTGTTATAGG	GAACCGGTGTACTCAAGAGC
blood	AAGACTGCCCTCGACCATTG	ATTCGCTGTTGTCATGTGCG
quasimodo	CCCGACAACAGACAAGAGGC	AGCCCAAGTGTTGCACTGTT
gypsy5	GCCCAGAGACAACGACAGAA	CTGTCTTTGCTGTCCCGGAT
17.6	AATTGGCGCAGTCGATGTGA	TGCCCGTTATCGTGGTACTT
mdg3	ATGCCATACGATGCGCAAAC	CGCTCTTCCTTGTGGGACAT